Photodynamic Therapy utilizing Interstitial Light Delivery Combined with Spectroscopic Methods

Marcelo Soto Thompson

Department of Physics

Till Elin
&
La Familia

Contents

Abstract

Since cancer continues to plague humanity there is large need for development of modalities for both diagnosis and therapy. Most of the currently available methods suffer from serious disadvantages. The treatments, e.g. ionising radiation, chemo-therapy, surgery, may themselves induce malignancies or the patient may be physically impaired for a longer period of time.

The work presented aims at developing equipment and methods that use light for both detection and treatment of various malignant or pre-malignant conditions. Fundamental knowledge on the interaction between light and tissue is required in order to develop models for the light distribution in tissue. Therefore, basic properties of light-tissue interaction, like refractive index, absorption, scattering, and scattering anisotropy, are introduced. How the physiological status of the tissue affects these properties are discussed.

Utilizing the differences in the fluorescence spectra emitted by healthy and malignant tissues, when irradiated with visible light, it is possible to detect and delineate certain lesions. The contrast between diseased and healthy tissue can be further enhanced with the use of a fluorescence tumour marker. The evolution of these tumour markers has been fuelled by the fact that many tumour markers also can be utilized for light therapy. The modality is called photodynamic therapy (PDT) and has now been clinically approved for the treatment of several conditions. The possible indications for this type of treatment are generally limited to thin superficial lesions due to the limited penetration of the light in tissue.

The work presented in this thesis mainly relates to overcoming the limited light penetration by leading the light through multiple optical fibres inserted into the tumour. In this way both embedded tumour and/or thick tumours could be an indication for this modality. In addition to that the fibres are used to collect information about relevant parameters of therapeutic interest.

Swedish summary/Sammanfattning

Redan för 5000 år sedan i det antika Egypten användes ljus för att behandla vissa hudåkommor. Denna bortglömda kunskap återupptäcktes i början av förra seklet men fick inget riktigt genomslag. De senare årtiondenas framsteg inom kemi och fysik har återigen gjort ljusbehandling av sjukdomar högintressant. Speciellt upptäckten av lasern på 1960-talet har gjort att tillämpningarna av ljus inom många medicinska områden fått ett kraftigt uppsving de senaste 20 åren. Denna avhandling handlar om att vidareutveckla en typ av metod för att hitta och bota cancer med hjälp av en tumörselektiv, ljuskänslig medicin som aktiveras med synligt ljus från t.ex. en laser. Utrustning för detta har utvecklats främst i Lunds Universitets regi men numera även i bolagsform, då under namnet SpectraCure.

Låt kroppen själv peka ut tumören!
På våra sjukhus hittar man numera lasrar på nästan alla avdelningar. För det mesta utnyttjas bara laserns egenskap att ge intensivt ljus för att skära eller bränna bort vävnad och samtidigt koagulera de blodkärl den skär igenom, likt en blödningsfri kniv. På senare tid har andra egenskaper gjort den idealisk även för behandlingar där den fungerar som katalysator i kemiska processer, så kallade fotokemiska processer. Vid dessa fotokemiska processer kan man på ett effektivt sätt utnyttja skillnader mellan friska celler och tumörceller för att låta lasern dels peka ut var tumören finns, och dels döda sjuka celler, samtidigt som man skonar omgivande friska celler. Det finns många olika ämnen som har någon egenskap som gör att de ansamlas mer i tumörceller än i friska celler.

Ett ämne som ger upphov till en sådan typ av ansamling är aminolevulinsyra (ALA) en aminosyra som är ett förstadium till hemoglobin (eller haem), det syretransporterande färgämnet i röda blodceller. Alla celler i kroppen tillverkar hemoglobin i högre eller lägre grad i den så kallade haemcykeln, se figur I. Processerna i haemcykeln sker relativt snabbt (ca en timme) utom det sista, långsamma, steget som tar cirka ett dygn. Detta sista steg består i att protoporfyrin IX (PpIX), som bildats ur ALA, binder järn till sig och blir haem och senare hemoglobin. Den generellt stegrade aktiviteten i tumörceller gör att dessa har en accelererad haemcykel jämfört med liknande friska celler. Genom att då ge patienten ALA och sedan vänta några timmar så får man en ungefär tre gånger högre koncentration av PpIX i tumörcellerna än i friska celler.
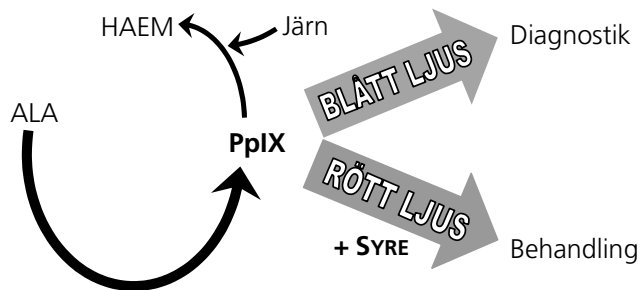
I. Skiss av haemcykeln samt effekten av belysning av PpIX med olika färg.

PpIX är ett ljuskänsligt ämne som vid belysning *fluorescerar* d.v.s. utsänder karakteristiskt ljus med en annan färg än den färg det belyses av. I fallet med PpIX får man en kraftig röd fluorescens (våglängd 635 nanometer) vid belysning med blått ljus (våglängd 405 nanometer). Om ett misstänkt område på en cancerpatient som tidigare fått ALA belyses det sättet kommer sjuk vävnad att avge mer rött ljus är frisk vävnad. På så sätt kan man avgränsa tumören på ett sätt som inte är möjligt med blotta ögat.

Självreglerande och intelligent ljusterapi

En annan gynnsam egenskap hos PpIX är att det är fotokemiskt aktivt. Vid belysning med rött ljus (av samma färg som fluorescensljuset) kommer PpIX att reagera med syret i cellerna och olika typer av fria radikaler. Dessa fria radikaler är starkt reaktiva och förstör i princip det första de stöter på. Detta sker vanligtvis inom den cell där de skapades, och vid tillräcklig hög koncentration kommer cellen att dödas. Återigen utnyttjar man alltså att det finns en större andel PpIX i cancercellerna, som därigenom kommer att lida större skada av ljuset än de intilliggande, friska cellerna. I den här processen bryts även PpIX ner, samtidigt som syret återgår till vanligt ofarligt syre. Hela processen blir därmed också självreglerande. Metoden heter fotodynamisk terapi (PDT eng. *Photodynamic therapy*) och har tre kritiska faktorer: halten av PpIX, syresättningen i tumören och mängden behandlingsljus.

Metodens för- och nackdelar

PDT kan med fördel användas på områden där det är viktigt att inte skada frisk vävnad av kosmetiska och medicinska skäl, till exempel i ansiktet eller på genitalierna. Metoden har ett snabbt läkningsförlopp (några veckor), och det går inte att överbehandla (som i fallet med behandling med radioaktiva preparat) utan behandlingen kan upprepas så många gånger man behöver.

II. PDT av patient med tumör på nästippen. Laserljuset levereras med hjälp av en optisk fiber, på bilden fastsatt på en vanlig undersöknings-lampa.

Patienten kan enkelt ges ALA antingen oralt (utblandat i juice), intravenöst eller ut-blandat i en kräm som smörjs in direkt på tumörområdet. Jämfört med traditionella cancerbehandlingar som kirurgi, radioaktiv strålning eller cellgifter orsakar metoden väsentligt mindre obehag för patienten. Även för personalen är metoden relativt okomplicerad och kräver bara ögonskydd. Den här typen av behandling sker regel-bundet på ett flertal sjukhus i Sverige idag, se figur II.

Metoden orsakar en lätt till måttlig smärta under de 5 till 10 minuter själva ljus-behandlingen tar, men det kan enkelt mildras genom att badda området med lite kallt vatten. En större nackdel är då behandlingsljusets begränsade inträngning i vävnad. För det röda behandlingsljuset räknar man ett effektivt behandlingsdjup på cirka 3 millimeter i vävnad. För det blåa detektionsljuset är samma siffra bara några tusendels millimeter! Detta begränsar användningsområdena för PDT till tunna och ytliga tumörer. Det kan även vara olämpligt att behandla vävnad som har naturligt hög produktion av hemoglobin som till exempel benmärg, lever och mag-tarmkanalen.

Interstitiell PDT enligt Lundamodellen

Ett sätt att komma runt problemet med att man bara kan behandla ytliga tumörer, skulle kunna vara att leda behandlingsljuset in i tumören via en optisk fiber som sticks ner i tumören, så kallad interstitiell PDT. Då skulle man kunna behandla en volym på cirka tre millimeter i radie kring fiberspetsen. Genom att sedan flytta runt fibern eller använda sig av flera fibrer skulle man kunna behandla *både* tjocka tumörer *och* tumörer som inte ligger ytligt. Interstitiell PDT förekommer i enstaka fall vid ett fåtal sjukhus i världen.

Vi har inom gruppen arbetat ett flertal år med att tillverka utrustning som bygger på att man använder sig av flera fibrer där man kan använda fibrerna för att ömsom behandla tumören och ömsom mäta ljuset från omgivande fibrer, se figur III. På så sätt kan man ta hänsyn till om ljusflödet i tumören skulle ändras drastiskt på grund av till exempel en blödning och då korrigera behandlingstiden. Man kan även mäta syresättningen igenom tumören på liknande sätt. Syresättningen är ju en kritisk faktor i behandlingen: Ingen syresättning – inga syreradikaler – ingen behandling. Om man dessutom mäter fluorescensen från PpIX via fibrerna har man kontroll på de tre kritiska faktorerna i behandlingen: PpIX-halten, syresättningen och mängden behandlingsljus.

III. Två nyutvecklade utrustningar för Interstitiell-PDT (vä, mitten). Interstitiell-PDT för behandling av en tjock tumör på vaden (hö).

Kommersiell vidareutveckling

Lunds Universitets Utvecklingsbolag (LUAB) vände sig under hösten 2002 till Karolinska Innovations AB (KIAB) för att se om man kunde samarbeta runt den utvecklade teknologin. Resultatet blev att LUAB och KIAB tillsammans med oss forskare bildade SpectraCure AB. Genom företaget utvecklas behandlingsstrategier för patienter med vissa typer av cancersjukdomar. På sikt skulle denna typ av behandling kunna bidra till ökad effektivitet i sjukvården med färre behandlingar och samtidigt erbjuda en säker och kontrollerad behandling med interaktiv återkoppling för bl.a. ljusdos-beräkningar. För närvarande pågår de första, mellan SpectraCure och Lunds Universitet, gemensamma kliniska behandlingarna på Universitetssjukhuset i Lund.

List of Papers

The thesis is based on the following papers:

I. Soto Thompson, M., Gustafsson, L., Pålsson, S., Bendsoe, N., Stenberg, M., af Klinteberg, C., Andersson-Engels, S. and Svanberg, K., Photodynamic therapy and diagnostic measurements of basal cell carcinomas using esterified and non-esterified δ-aminolevulinic acid, *J. Porphyrines Phthalocyanines*, **5**, 147-153 (2001).

II. Pålsson, S., Gustafsson, L., Bendsoe, N., Soto Thompson, M., Andersson-Engels, S. and Svanberg, K., Kinetics of the superficial perfusion and temperature in connection with photodynamic therapy of basal cell carcinomas using esterified and non-esterified 5-aminolevulinic acid, *Br. J. Dermatol.,* **148**, 1179-1188 (2003).

III. Soto Thompson, M., Johansson, T., Pålsson, S., Andersson-Engels, S., Svanberg, S., Bendsoe, N., Stenram, U., Svanberg, K., Spigulis, J., Derjabo, A. and Kapostins, J., Photodynamic therapy of basal cell carcinoma with multi-fibre contact light delivery, Submitted (2004).

IV. Pålsson, S., Gustafsson, L., Stenram, U., Soto Thompson, M., Svanberg, S., Svanberg, K. and Andersson-Engels, S., Estimation of the protoporphyrin IX photodynamic threshold dose, Submitted (2003).

V. Stenberg, M., Soto Thompson, M., Johansson, T., Pålsson, S., af Klinteberg, C., Andersson-Engels, S., Stenram, U., Svanberg, S. and Svanberg, K., Interstitial photodynamic therapy - Diagnostic measurements and treatment in malignant experimental rat tumours, in *Optical Biopsy and Tissue Optics*, eds. Bigio, I.J., Mueller, G.J., Puppels, G.J., Steiner, R.W., and Svanberg, K., Proc. SPIE, vol. **4161**, 151-157 (2000).

VI. Johansson, T., Soto Thompson, M., Stenberg, M., af Klinteberg, C., Andersson-Engels, S., Svanberg, S. and Svanberg, K., Feasibility study of a novel system for combined light dosimetry and interstitial photodynamic treatment of massive tumors, *Appl. Opt.,* **41**, 1462-1468 (2002).

VII. Soto Thompson, M., Johansson, A., Johansson, T., Andersson-Engels, S., Bendsoe, N., Svanberg, K. and Svanberg, S., Clinical system for interstitial photodynamic therapy with combined on-line dosimetry measurements, Submitted (2004).

VIII. Pålsson, S., Stenram, U., Soto Thompson, M., Vaitkuviene, A., Poskiene, V., Ziobakiene, R., Oyama, J., Bendsoe, N., Andersson-Engels, S., Svanberg, S. and Svanberg, K., Methods for detailed

histopathological investigation and localisation of cervical biopsies to improve the interpretation of autofluorescence data, Submitted (2003).

IX. Gustafsson, U., McLaughlin, E., Jacobson, E., Håkansson, J., Troy, P., DeWeert, M.J., Pålsson, S., Soto Thompson, M., Svanberg, S., Vaitkuviene, A. and Svanberg, K., Fluorescence and reflectance monitoring of human cervical tissue in vivo - A case study, in *Spectral imaging: Instrumentation, applications, and analysis II*, eds. Levenson, R.M., Bearman, G.H., and Mahadevan-Jensen, A., Proc. SPIE vol. **4959**, 100-110 (2003).

X. DeWeert, M.J., Oyama, J., McLaughlin, E., Jacobson, E., Håkansson, J., Bignami, G.S., Gustafsson, U., Troy, P., Poskiene, V., Kriukelyte, K., Ziobakiene, R., Vaitkuviene, A., Pålsson, S., Soto Thompson, M., Stenram, U., Andersson-Engels, S., Svanberg, S. and Svanberg, K., Analysis of the spatial variability in hyperspectral imagery of the uterine cervix in vivo, in *Spectral imaging: Instrumentation, applications, and analysis II*, eds. Levenson, R.M., Bearman, G.H., and Mahadevan-Jensen, A., Proc. SPIE vol. **4959**, 67-76 (2003).

Additional material has been presented in

XI. Soto Thompson, M. Intelligent metod hittar och botar cancer, (2003).

XII. Soto Thompson, M., Andersson-Engels, S. and Svanberg, S., System and method for therapy and diagnosis comprising optical components for distribution of radiation., Swedish patent application No. 0301411-5, U.S. patent application No. PCT/SE2004/000756, (2003).

XIII. Johansson, T., Eker, C., Malmborg, J., Wesseltoft Mogensen, L., Svanberg, S., Soto Thompson, M. and Andersson-Engels, S., System and method for therapy and diagnosis comprising translatory distributor for distribution of radiation., Swedish patent application No. 00301406-5, U.S. patent application No. PCT/SE2004/000755, (2003).

XIV. Johansson, A., Andersson-Engels, S., Johansson, T., Pålsson, S., Soto Thompson, M., Svanberg, K. and Svanberg, S., System and method for therapy and diagnosis comprising optical and mechanical distributors for distribution of radiation., Swedish patent application No. 0301411-5, U.S. patent application No. PCT/SE2004/000758, (2003).

XV. Andersson-Engels, S., Bendsoe, N., Johansson, T., Pålsson, S., Soto Thompson, M., Stenram, U., Svanberg, K. and Svanberg, S., Integrated system for interstitial photodynamic therapy, in *Advanced Optical Devices*, eds. Spigulis, J., Teteris, J., Ozolinsh, M. and Lusis, A., Proc. SPIE vol. **5123**, 293-302 (2003). Invited.

XVI. Andersson-Engels, S., Bendsoe, N., Johansson, A., Johansson, T., Pålsson, S., Soto Thompson, M., Svanberg, K. and Svanberg, S., Integrated system for interstitial photodynamic therapy, in *Therapeutic*

Laser Applications and Laser-Tissue Interactions, ed. Steiner, R., Proc. SPIE vol. **5142**, 42-48 (2003).

XVII.   Gustafsson, U., McLaughlin, E., Jacobson, E., Håkansson, J., Troy, P., DeWeert, M.J., Pålsson, S., Soto Thompson, M., Svanberg, S., Vaitkuviene, A. and Svanberg, K., In-vivo fluorescence and reflectance imaging of human cervical tissue, in *Medical imaging 2003: physiology and function: methods, systems, and applications*, eds. Clough A.V. and Amir, A.A., Proc. SPIE vol. **5031**, 521-530 (2003).

Presentations given,

XVIII.   Soto Thompson, M., Gustafsson, G., Pålsson, S., Bendsoe, N., Stenberg, M., af Klinteberg, C., Andersson-Engels, S., Svanberg, K., Photo-dynamic therapy and diagnostic measurements of basal cell carcinomas using esterified and non esterified 5-aminolevulinic acid, ICPP1, Dijon, France, (2000).

XIX.   Soto Thompson, M., Interstitial PDT- fibre guided laser treatment of tumours, BIOP , Risoe, Denmark, (2000)

XX.   Soto Thompson, M., Stenberg, M., Johansson, T., Pålsson, S., af Klinteberg, C., Andersson-Engels, S., Svanberg, S., Svanberg, K., Novel system for integrated interstitial photodynamic therapy, dosimetry measurements and prediction of treatment outcome, WCPM-8, Vancouver, BC, Canada, (2001).

XXI.   Soto Thompson, M., Stenberg, M., Johansson, T., Pålsson, S., af Klinteberg, C., Andersson-Engels, S., Svanberg, S., Svanberg, K., Novel system for integrated interstitial photodynamic therapy; dosimetry measurements and treatment outcome, ECBO, Munich, Germany (2001).

XXII.   Soto Thompson, M., Laser-based spectroscopy in the treatment and diagnostics of cancer. 1st German-Swedish workshop on "Physics in Medicine and Bioanalysis", Berlin, Germany, (2002)

XXIII.   Soto Thompson, M., Zhao, H., Swartling, J., Andersson-Engels, S., Dosimetry and fluence rate calculations for fiber-guided interstitial photodynamic therapy; tissue phantom measurements and theoretical modelling, Photonics West, San Jose, USA, (2003).

List of symbols and abbreviations

Listed below are the symbols abbreviations, and terms used throughout the thesis, were applicable with the unit used within brackets.

Symbols

ε	molar extinction coefficient, [m^2/mol]
$\phi(\mathbf{r},t)$	fluence rate, [mW/cm^2]
λ	wavelength, [nm]
μ_a	absorption coefficient, [cm^{-1}]
μ_{eff}	effective attenuation, $\sqrt{3\mu_a(\mu_a + \mu_s')}$, [$cm^{-1}$]
μ_s	scattering coefficient, [cm^{-1}]
μ_s'	reduced scattering coefficient, $\mu_s(1\text{-}g)$, [cm^{-1}]
μ_{tr}	transport coefficient, $\mu_{tr} = \mu_a + \mu_s(1\text{-}g)$, [$cm^{-1}$]
ω	solid angle, [sr]
θ	plane angle, [radians, °]
c	speed of light, [299 792 458 m/s, by definition]
D	diffusion coefficient, $1/3(\mu_a+\mu_s')$, [cm]
$E(\mathbf{r},t)$	irradiance, [W/m^2]
f	frequency, [Hz, 1/s]
$\mathbf{F}(\mathbf{r},t)$	photon flux, [W/m^2]
g	anisotropy factor, $g = \langle\cos\theta\rangle$
h	Planck's constant, [6.63 10^{-34} Js]
$\mathbf{k}$	wave vector, $2\pi/\lambda\cdot\mathbf{s}$, [1/m]
$L(\mathbf{r},\mathbf{s},t)$	radiance, [W/m^2sr]
n	refractive index
$N(\mathbf{r},\mathbf{s},t)$	photon distribution function, [1/m^3sr]
$p(\theta)$	scattering phase function
$q(\mathbf{r},t)$	source term, [W/m^3]
$Q(\mathbf{r},t)$	source term, [W/m^3 sr]
$\mathbf{r}$, r	position: 3- and 1-dimensions, respectively, [m]
R	reflected intensity, [W]
$\mathbf{s}_i$, $\mathbf{s}_s$	unit vector of incident and scattered light, respectively
t	time, [s]
$\mathbf{v}$, v	velocity vector, speed (v=c/n), [m/s]
$W(\mathbf{r})$	deposited light dose at position $\mathbf{r}$, $W(\mathbf{r}) = \mu_a \int \phi(\mathbf{r},t)dt$, [J/$m^3$]

Abbreviations

ALA	aminolaevulinic acid
ALA-ME	methyl-esterified ALA, also m-ALA, Metvix®
BCC	basal cell carcinoma
BPD	benzoporphyrin derivative, Visudyne®
D	diffusion coefficient, $1/3(\mu_a+\mu_s')$, [cm]
DE	the time-independent diffusion equation
FEM	Finite Element Method
Hb	deoxygenated haemoglobin
HbO$_2$	oxygenated haemoglobin
HpD	haematoporphyrin derivative
in vivo	literally: "in the living"
IPDT	interstitial photodynamic therapy
IR	infrared
LDPI	laser Doppler perfusion imaging
LIF	laser-induced fluorescence
mTHPC	meta-tetrahydroxyphenylchlorin, also Temoporfin, Foscan®
PDT	photodynamic therapy
PpIX	protoporphyrin IX
RTE	radiative transport equation
SC	*stratum corneum*, the outermost layer of the skin
UV	ultraviolet

Chapter 1

Introduction

Sunlight is fundamental to all kinds of life, in one way or another. The sun propels the main biochemical process, the photosynthesis, which leads to the widespread vegetation flourishing all over. In this case sunlight interacts with the chlorophyll in the green plants transforming carbon dioxide and water into carbohydrates and oxygen, which in turn both are prerequisites for all animal life. In our body the sun induces a similar biochemical process when synthesising vitamin D_3 after absorption of ultraviolet light in the skin. The same kind of light also produces a different response in the melanosomes in the skin. Here, the radiation stimulates the production of melanin, the dark pigment in the skin, that will eventually stop the UV light from penetrating further down into the skin. But perhaps the most fascinating light-tissue interaction is our ability to perceive visible light with our eyes, see Fig. 1[1,2].
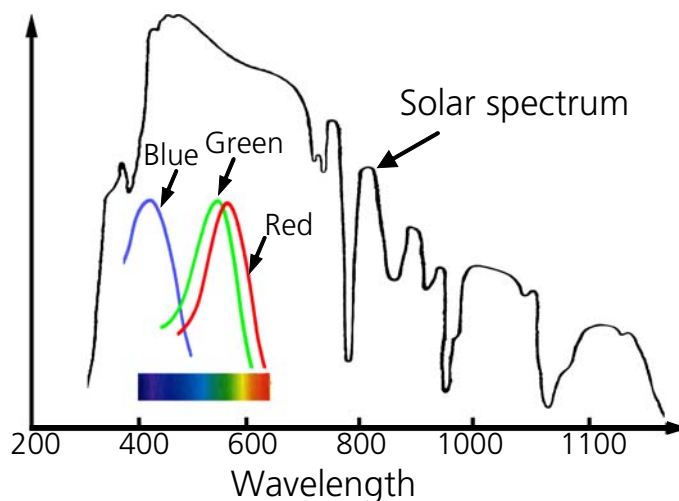

Fig. 1. The intensity of the sunlight reaching the earth along with the colour sensitivity of the eye, adapted from Svanberg[1] and Vander[2].

Not only do we possess a system for detection of light that can span from the faintest glimmer to the high levels of light on a sunny summer day but our colour vision is also perfectly matched to daylight conditions. The total sensitivity of our eyes is at its highest for the interval that is the most intense of the sun at noon. These examples illustrate some of the varieties, and complexities, of the interactions between light and tissue.

This thesis will focus on a completely different aspect of light and tissue interaction. The common denominator to the examples given above is the interaction between light and biological media. In Chapter 2 the fundamental physical and physiological background to light-tissue interaction is introduced. Chapter 3 presents the most common mathematical theories used to model light distribution in tissue, with emphasis on the models used within the framework of the thesis. Chapter 4 deals with fluorescence spectroscopy and its use within the field of medicine. The explanation to the features of tissue fluorescence is discussed, presented along with different types of equipment. Also, aspects on how to interpret fluorescence spectra are discussed. Chapter 5 deals with photodynamic therapy (PDT), a tumour targeting treatment that, historically, has been developed in parallel with fluorescence spectroscopy. Finally, Chapter 6 deals with interstitial PDT (IPDT), a modality within the field of PDT aiming at expanding the possible indications for PDT through interstitial light delivery. Much of the work behind this thesis was performed in order to develop methods, to improve and develop equipment, and to strive making IPDT a serious clinical alternative.

Chapter 2

Interaction of light with tissue

This chapter will introduce the basic concepts of light-tissue interaction in the visible, near infrared (IR) region and the ultraviolet (UV) region. The major interaction processes, absorption and scattering, will be discussed in more detail especially the physiological properties governing light propagation will be explained.

2.1   Properties of light

The term light generally relates to the portion of the electromagnetic (EM) spectrum that we can see by the naked eye, having wavelengths between approximately 400 nm and 700 nm, represented by the shaded area in Fig. 2. In the Fig. various units for the energy of a photon are presented. For the purpose of this thesis the term *light* will be extended to refer also to the regions of the UV and IR closest to the visible region.
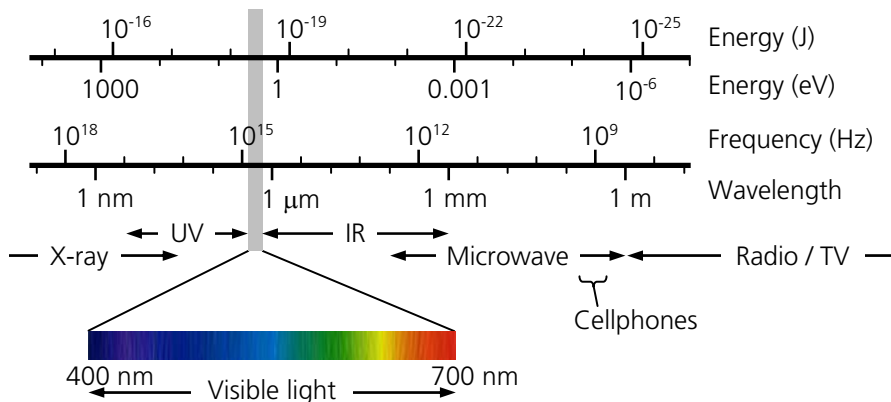

Fig. 2. Part of the EM spectrum in various common units.

The relation between the different energy units can be expressed as:

$$E(J) = hf(Hz) = \frac{hc}{\lambda(m)} = E(eV) \cdot q_e, \tag{1}$$

where h denotes Planck's constant (6.6 10^{-34} Js), f the frequency in hertz, c the speed of light (3.0 10^8 m/s) and λ the wavelength in metres. The energy in joules, E(J), scales to the energy in eV, E(eV), by the electron unit charge, q_e (1.6 10^{-19} C).

Light can be fundamentally described as a photon - having either wave or particle properties. For most practical applications describing light as a propagating photon is the most straight-forward approach although this description cannot fully explain some phenomena, such a diffraction, polarisation and interference (see Sect. 2.2.3). Unfortunately, tissue is a highly scattering media, which makes the description of light-tissue interaction very complex. Much effort is being put into developing models on how to model light propagation in tissue. Below is the background to the methods used in the work are presented.

2.2   Light propagation in tissue

Many different processes can take place when light interacts with matter. The process that will actually occur will depend on the intensity of the light, the wavelength of the light, and what kind of matter it interacts with. For the scope of this thesis we will focus on the most likely events within the field of tissue optics, see Fig. 3. In general, light will interact with the outermost electrons of the molecule it impinges onto. When interacting with the electrons basically two processes may occur; the photon may be absorbed or it may be scattered. Within tissue optics, absorption is commonly quantified by the absorption coefficient μ_a, which is defined as the probability for a photon to be absorbed per unit length, often given in cm^{-1} or mm^{-1}. If the energy of the photon does not match the difference between the energy levels in the molecule the photon might get scattered. For a scattering event the direction of the photon will (likely) change and the photon might or might not change its energy: *inelastic* or *elastic* scattering, respectively. The time scale of scattering is in the order of femtoseconds (10^{-15} s). Inelastic scattering is the basis for Raman spectroscopy, which has been successfully used for tissue characterization[3-5]. In tissue, the elastic scattering is several orders of magnitudes stronger than the inelastic scattering, thus for the remainder of this thesis the term scattering will mainly refer to elastic scattering. Scattering will be addressed in more detail in Sect. 2.2.3. The scattering is quantified in a similar manner as the absorption by a scattering coefficient μ_s, defined as the probability for a scattering event to occur per unit length. Also the directivity of the scattering, often quantified by the anisotropy factor g, has to be considered, see Sect. 2.2.3.
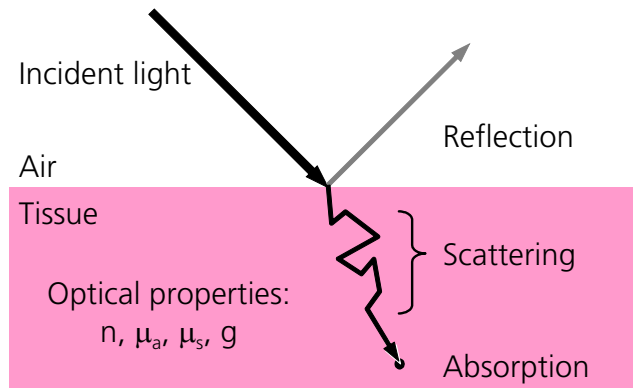
Fig. 3. Fundamental events in light-tissue interaction. By knowing the (wavelength-dependent) optical properties of the tissue type it is somewhat possible to predict the light distribution.

Considering absorption, the energy of the photon matches the difference between the energy levels in the molecule. Then the photon might get annihilated, transferring its energy to one of the electrons of the molecule, see Fig. 4. The electron is thereby transferred from the ground state to some excited state. The excited molecule now has several ways to relax back to the ground state. Perhaps the most obvious way for the molecule to relax would be to return to the original level emitting a photon of the same energy as the incoming photon, not necessarily in the same direction. This is in principle the same as scattering, although absorption is not a prerequisite for scattering. The excited molecule may also lose some energy by internal conversion (IC, indicated by the wavy black arrow in Fig. 4), which is a non-radiative process generating heat. By internal conversion the molecule will eventually end up in the lowest level in the excited state from where it can decay back to some of the levels of the ground state (within a time order of nanoseconds) under emission of fluorescence light. More frequently the molecules return to the ground state in collisional processes not emitting light, but generally heat. Since the energy levels for a molecule are not discrete as they would be for a simple free atom (illustrated by the horizontal lines in the Fig.) but rather consist of a continuum of levels (shaded area), the fluorescence spectrum generally consist of many indistinguishable lines giving a smooth, albeit, characteristic spectrum. In addition to that, for some "exotic" molecules there are some transitions that are more probable resulting in typical peaks in the spectrum. The phenomenon of fluorescence and fluorescence spectroscopy for medical purposes is further described in Chapter 4.
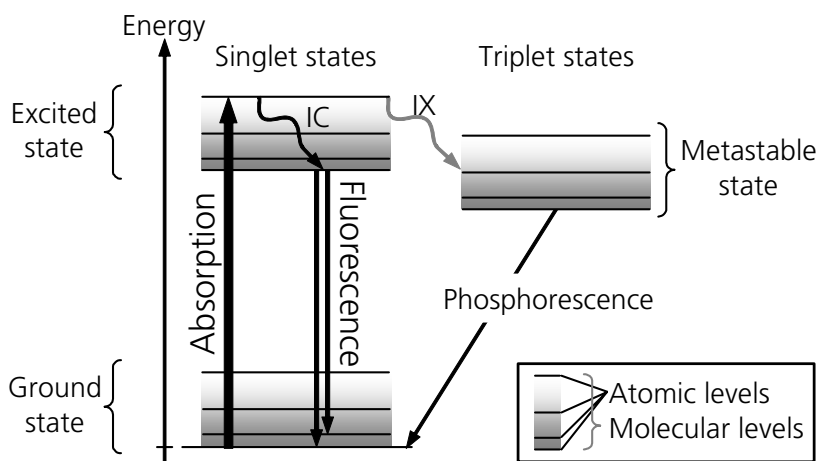
Fig. 4. Energy level diagram illustrating some possible pathways of light-matter interaction after absorption of a photon. Normally for a photon to interact with an atom or molecule the energy of the photon has to coincide with the energy difference between two possible configurations of the atom or molecule. These configurations result in two energy levels. For free atoms the levels are discrete while for molecules, solids or liquids the many levels many vibrational and rotational levels smear into a continuum. The internal conversion (IC) is a non-radiative process (here only shown in the excited singlet state) competing with all other decay processes. The "forbidden" intersystem crossing (IX) leads to metastable molecules and emission of phosphorescent light.

Quantum mechanical considerations state that the angular momentum of the molecule system has to be preserved, meaning that certain selection rules prevail and optically allowed transitions can only occur within the same multiplicity, i.e. total electron spin, "singlet to singlet, triplet to triplet". However, the "forbidden" intersystem crossings (IX, singlet to triplet transitions), illustrated by the grey arrow in Fig. 4, actually do have a slight possibility to occur in more complex molecules. Since the final relaxation between the triplet excited state down to the singlet ground state is fairly unlikely, although possible, the molecule will remain in the excited, *metastable*, triplet state for a long time (~μs-s) before emission of phosphorescent light. During the time in the metastable state the molecule may instead undergo collisions with other neighbouring atoms or molecules, subsequently transferring its excess energy to these. This energy transfer is fundamental for photodynamic therapy (PDT), further described in Chapter 5.

2.2.1 Tissue absorption

The relation between the concentration of tissue constituent, C_X [mol/dm^3], and the corresponding absorption coefficient, $\mu_a^\lambda(X)$, at a certain wavelength, λ, is given by[6]:

$$\mu_a^\lambda(X) = \ln(10) \cdot \varepsilon_X^\lambda \cdot C_X, \tag{2}$$

where the product $\varepsilon_X^\lambda \cdot C_X$ is defined in units of cm^{-1}, ε_X^λ is the molar extinction coefficient. Tissue absorbers are commonly referred to as *chromophores*.

In Fig. 5 the absorption coefficients of some major chromophores are shown, from the pioneering work of Boulnois[7]. The grey area in the Fig., between approximately 630 nm to 1300 nm indicates where the tissue constituents have their lowest overall absorption. This region is generally called *the tissue optical window*, referring to the possibility to penetrate deeply with light into tissue.
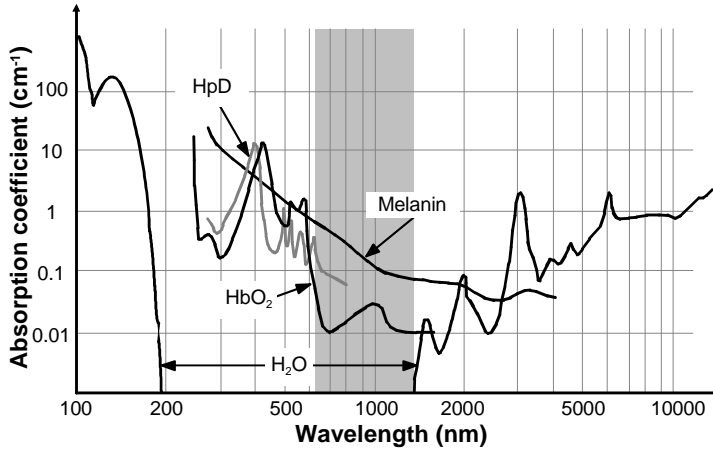
Fig. 5. The absorption as a function of wavelength of some of the most prominent chromophores in tissue. Note the logarithmic scale on the y-axis. The shaded area is referred to as *the optical window* due to a low total absorption (Figure adapted from Boulnois[7]).

In the UV- and the IR-region above approximately 1400 nm, the high specific absorption along with the mostly high contents of water in tissue makes water the dominant absorber. Minor absorption peaks also are also present at 975 nm, 1200 nm and 1440 nm[8]. The high absorption of water in the IR and UV along with the available high intensity lasers in those ranges (CO$_2$: 10600 nm, Excimer: 193 nm) has lead to the common use of lasers for surgical tissue cutting, tissue ablation and corrective laser eye surgery, LASIK.

Melanin is the chromophore that gives us the colour of the skin, hair and iris in the eye. In the blue/UV-region the melanin in the skin absorbs the most, protecting the skin below from the rays of the sun. Melanin in its pure form is extremely absorbent and cannot be extracted from the melanosome without changing its optical properties, which makes the measurement of its absorption coefficient very uncertain[9]. Jacques and MacAuliffe have presented an approximate empirical formula for the absorption coefficient of melanin[9]:

$$\mu_a = 1.70 \cdot 10^{12} \lambda^{-3.48} \text{cm}^{-1}, \tag{3}$$

with λ inserted in units of nm. In many cases the melanin layer is very thin and can often be modelled as a grey filter. For some conditions, such as malignant melanoma, the high concentration of melanin makes them virtually impenetrable to light.

The absorption in the internal organs is dominated by the very high absorption in haemoglobin. Haemoglobin is the oxygen carrying protein in the red blood cells, responsible for the oxygen transport from the lungs to the tissue. Haemoglobin is made up of four haem groups with an iron atom in the centre acting as the oxygen binding site. For haemoglobin the absorption will vary depending on if the haemoglobin is oxygenated (HbO_2) or not (Hb); see Fig. 6[10]. The absorption is at its highest for the so-called *Soret band*, at 414 nm and 433 nm for HbO_2 and Hb, respectively. It then drops off steeply until approximately 530 nm, where it picks up slightly again at the *Q-band* (with two typical peaks for HbO_2 at 540 nm and 576 nm). The lowest absorption is found for wavelengths above 600 nm. For several wavelengths, e.g. 500, 530, 545, 570, 584, and 797 nm, the absorption of HbO_2 is equal to the absorption of Hb. These, so-called *isobestic points*, can be used as reference for tissue oxygenation measurements. By measuring the transmittance at, e.g., 900 nm and 797 nm and forming the ratio between the transmittances one can monitor changes in tissue oxygenation. This is the basics of optical pulse oximetry and the theory behind the method is also utilized in the system developed for interstitial PDT (IPDT) presented in Chapter 6 and Paper VII.

In skeletal muscle tissue, myoglobin is the most abundant oxygen carrying protein and also serves as oxygen storage compartment. Myoglobin basically shares the spectral features of hemoglobin[11,12]. Typically the ratio between myoglobin and haemoglobin concentration in muscle tissue is 10:1, while haemoglobin is the only haem protein in other tissues[12]. Myoglobin consists of one single haem group, each one with an oxygen-binding iron atom. One physiological difference between these oxygen carrying proteins is that myoglobin remains almost fully oxygenated even at very low oxygen partial pressure while the saturation of haemoglobin depends more linearly on the oxygen partial pressure[2,13].
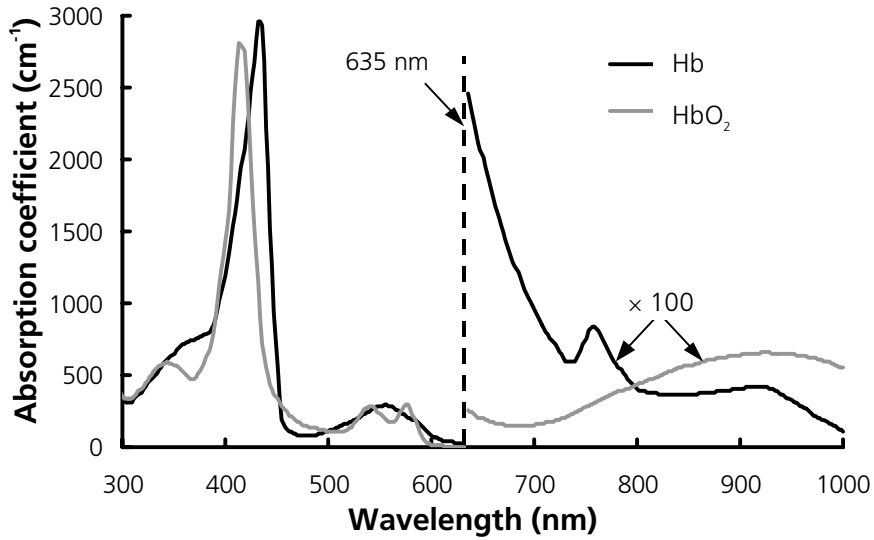
Fig. 6. The absorption spectra of Hb and HbO₂, at a concentration of 150 g/l of blood, compiled data from many sources by Prahl[10].

Included in Fig. 5 is also the spectrum of haematoporphyrin derivative (HpD). This is one of the first light sensitive compounds used for PDT. It is chemically similar to haemoglobin in that it has a porphyrin core, which gives it a typical spectrum. It has the highest absorption of the *Soret* band at about 400 nm and Q-band absorption with several peaks at 480-650 nm. The photosensitizers (used in Papers I-VII) δ-aminolaevulinic acid (ALA) and its successor methyl-esterified ALA (ALA-ME), will eventually induce protoporphyrin IX (PpIX), which also has this characteristic porphyrin core, c.f. Sect. 4.4.1.

2.2.2 Reflection at a tissue interface

When light passes an interface between two media of different refractive indices (typically air-tissue) a certain amount of the light will be reflected. This reflection will depend heavily on the polarisation of the light, the incident angle (θ_a), and the structure and shape of the medium; see Fig. 7a. In tissue optics the polarisation of the light can most often be neglected, unless the light is laser light delivered directly onto the tissue surface without the aid of optical fibres. By assuming a plane interface (neglecting the roughness of the tissue) then the reflection is governed by $\theta_a = \theta_r$, and the angle of refraction is given by Snell's law[14]:

$$n_a \sin\theta_a = n_t \sin\theta_t \tag{4}$$

Further, by utilising Fresnel's equations the reflected intensity R can be written as:

$$R = \frac{1}{2}\left[\frac{\tan^2(\theta_a - \theta_t)}{\tan^2(\theta_a + \theta_t)} + \frac{\sin^2(\theta_a - \theta_t)}{\sin^2(\theta_a + \theta_t)}\right] = \left.\left(\frac{n_a - n_t}{n_a + n_t}\right)^2\right|_{\theta=0}, \tag{5}$$

where the last step is derived by using Eq. (4) and assuming a perpendicular illumination ($\theta_a = \theta_t = 0°$). On a macroscopic level, most tissue types have an average refractive index in the range of 1.38-1.41[15,16] with the exception for adipose (fatty) tissue where it is about 1.46. At an air-tissue interface the reflection will be approximately 3% ($n_{air}=1$), which might not seem much.

We arrive at a more interesting consequence of the reflection by reversing the direction of the transmitted light as shown in Fig. 7b. At the limit of internal reflection, where θ_a equals 90° in Eq. (4), the angle ($\theta_{t, critical}$) of the light inside the tissue is approximately 46°. Light with a larger incidence angle will then be totally reflected at the tissue-air boundary. Since light will be very much scattered around in all directions, once it has entered the tissue, a great portion of the light will be reflected at the surface - trapped inside the tissue. Therefore, when illuminating an air-tissue boundary, the fluence rate just below the tissue surface will be several times higher than the incident fluence rate, depending on the diameter of the incident light[17].
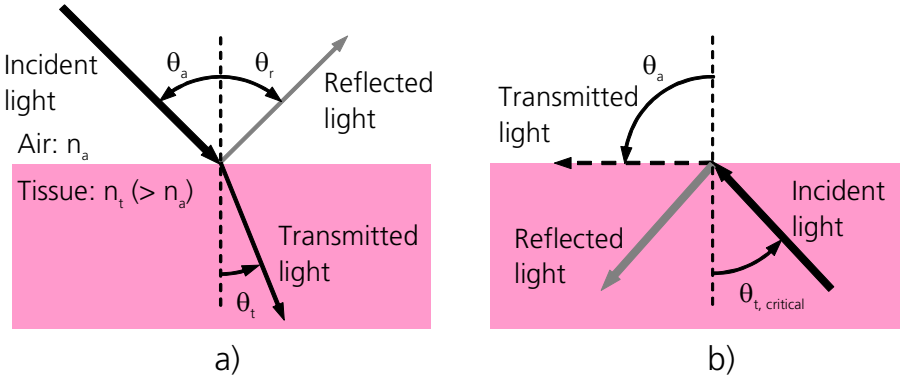

Fig. 7. a) The reflection of incident light at an interface (typically air-tissue) with higher refractive index in the second medium. b) Illustration of total internal reflection. For an incident angle larger than $\theta_{t, critical}$ all incident light will be reflected.

2.2.3 Scattering

So far we have looked at macroscopic reflections at an air-tissue interface that is quite easy to model. A much more complex scattering occurs on a microscopic scale where there will be multiple reflections between and within cells and organelles. The principal scatterers are the cell membranes[18], cell nuclei, mitocondria[19], the Golgi apparatus and lysosomes. In fatty tissue also the lipid vesicles contribute to the scattering[20], which in this case is temperature dependent[21]. Even if the cell membranes have a high refractive index (1.48) it has been shown that the membranes contribute quite little to the total scattering[22]. A suggested explanation to this is that although the organelles have a refractive index close to the that of the surrounding cytosol they are heavily folded (Golgi apparatus, endoplasmic reticulum) or contain folded structures (mitochondria) resulting in the high total scattering. As can be seen in Fig. 8 the scattering is much higher than the absorption in the optical window.
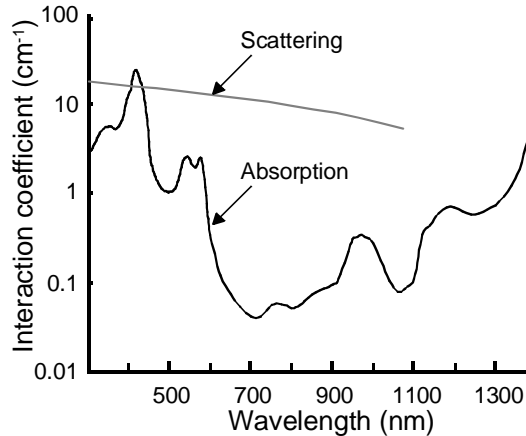
Fig. 8. Typical scattering and absorption coefficients for tissue, modified from af Klinteberg[23]. The absorption is a theoretical curve made up by combining the spectra for haemoglobin (1/3 Hb, 2/3 HbO$_2$, 1% w/w) and water (70% w/w)[10]. The scattering (μ'_s; compare Eq. (7)) is roughly 10-100 times stronger, than the absorption for nearly the whole of the optical window.

Looking at the scattering from a physicist's point of view there are mainly two kinds of approaches to theoretical modelling of scattering events: Rayleigh and Mie theory. The scattering obeys the Rayleigh model when light gets scattered by particles, the size of which is considerably smaller than the wavelength of the light.

The intensity of the Rayleigh scattered light follows a $1/\lambda^4$ dependence and it is isotropically distributed. Mie scattering is deduced by solving the well−known Maxwell's equations[i] for spherical particles when the size of the scatterers is comparable to the wavelength. The complexity of this approach only makes it possible to solve the equations for simple geometries. For Mie scattered light, the scattering is approximately proportional to $1/\lambda^2$, depending on the size of the scatterer, and it is highly peaked in the forward direction. The dependence of wavelength for the scattering types can be seen in Fig. 8 as the slope of the scattering curve is slightly flatter towards shorter wavelengths (where the Mie scattering is dominant) as compared to longer wavelength where the slope of the curve is steeper (and the Rayleigh scattering dominates).

Scattering anisotropy

Since tissue is not made up of randomly distributed cells, but rather consists of layered structures, such as skin, muscle fibres, blood vessels etc., it is not difficult to imagine that this might influence the scattering. The scattering in tissue has been shown to be very much forward scattering[24,25] and this has to be considered when modelling. A normalized scattering phase function p(**s**,**s'**) is then defined as being the probability for a photon to be scattered from the incoming direction **s** to a scattered direction **s'**; see Fig. 9a. The most commonly used phase function is the Henyey-Greenstein function[ii] since it agrees quite well with measured angular distributions[26] and has a simple analytical form. It can be written:

$$p(\cos\theta) = p(\mathbf{s} \cdot \mathbf{s'}) = \frac{1 - g^2}{4\pi\left(1 + g^2 - 2g\cos\theta\right)^{3/2}} \,, \tag{6}$$

The scattering anisotropy g, or g-factor, is introduced as the mean value of $\cos\theta$: $g = \langle\cos\theta\rangle$. The g-factor ranges between -1 and 1 for totally back scattering and totally forward scattering media, respectively, while g is equal to zero for an isotropically scattering medium; see Fig. 9b. For tissue the g-factor is typically about 0.8-0.95[27].

---

[i] James Clerk Maxwell (1831-79). Scottish physicist, considered to be one of the greatest ever. One of the founders of the electromagnetic wave theory. His work also includes major contributions in the field of thermodynamics.

[ii] Originally used for describing light scattering by interstellar dust clouds.
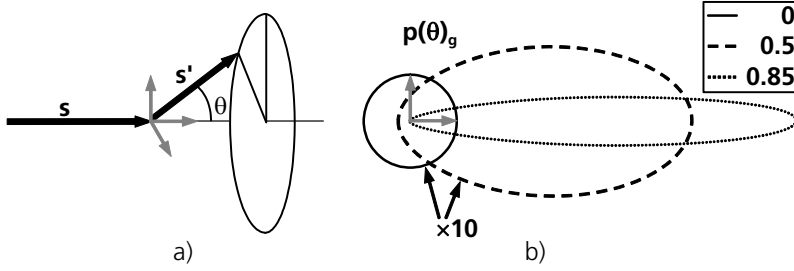
Fig. 9. a) Definitions of scattering vectors and angles b) Radial plots of the Henyey-Greenstein function for different values of the g-factor.

Following the definition of the anisotropy factor another quantity is often introduced; the reduced scattering coefficient μ_s':

$$\mu_s' = (1-g)\mu_s, \tag{7}$$

Keeping in mind that $1/\mu_s$ is the distance between subsequent scattering events with a scattering distribution determined by p(θ), then $1/\mu_s'$ is the distance of subsequent scattering events with virtual isotropic scattering; see Figure 10. A photon in a non−isotropically scattering medium can be thought of as being isotropically scattered after a distance of $1/\mu_s'$, or heuristically, a photon in a non−isotropically scattering media has lost track of its initial direction after a distance of $1/\mu_s'$.
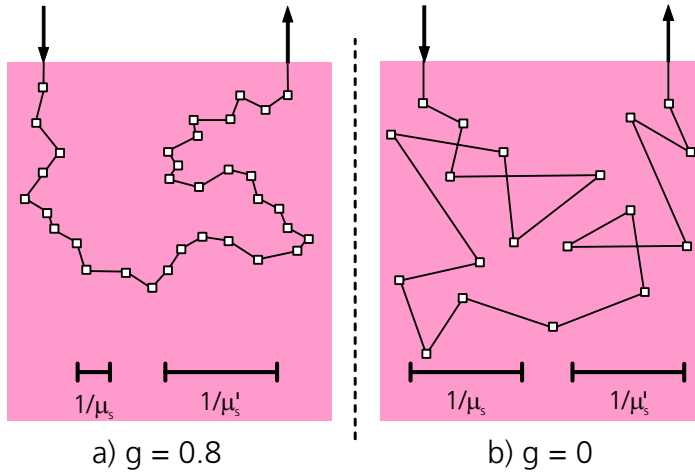
Figure 10. Simulated photon trajectories in a) a forward scattering medium (g = 0.8) and b) an isotropically scattering medium. The reduced scattering coefficient is the same in both figures though. Adapted from Swartling[28]

By knowing the full set of the optical properties (n, μ_a, μ_s and g) it is possible to make quite accurate predictions of the light flux in tissue. For many measurements of light in tissue at relatively long distances from the source, the light has become diffuse and lost track of its initial direction. It is then not possible to separate μ_s and g. This has led to the development of models relying on μ_s' and μ_a as tissue parameters, e.g. diffusion theory.

Laser Doppler shifted scattering

A special case of scattering occurs when the incident light gets scattered by moving cells e.g., blood cells. There will be a slight, however detectable, shift of the frequency (Δf) due to the Doppler effect[iii]:

$$\Delta f = \frac{v_{cell}}{c} f_0 \, , \tag{8}$$

where v_{cell} is the speed of the scattering cell and c is the speed of light, f_0 is the original light frequency. Since the speed of the blood is of the order of 10^{-3} m/s (in the capillaries) and the speed of light is $3.0 \cdot 10^8$ m/s, the ratio of the shift to the original frequency is only about 10^{-11}! Still it is possible to measure flows from 10^{-5} m/s up to 10 m/s. The frequency shift at a single scattering event is also dependent of the angles of the scattering according to[29]:

$$\Delta f = \frac{1}{2\pi} \left(\mathbf{k}_s - \mathbf{k}_i \right) \cdot \mathbf{v}_{cell} \, , \tag{9}$$

where $\mathbf{k}_s$ and $\mathbf{k}_i$ are the wave vectors of the scattered and incident photon, respectively, and $\mathbf{v}$ is the velocity vector of the scattering object. Since the light inside the tissue and the scattering objects are moving in many directions and the scattering objects move with different velocities, the detected signal will be a distribution of frequency shifts. By monitoring the frequency shift spectrum it is possible to assess the blood flow (or perfusion) *in vivo*.

The modality has been widely employed for both invasive point monitoring[30-32] as well as in a non-invasive imaging mode [33,34]. In Papers I and II a commercial imaging instrument[35] (Lisca Development AB, Linköping, Sweden) was used to measure perfusion changes in connection to PDT of superficial BCC. The system

---

[iii] Discovered by Austrian physicist Johann Christian Doppler (1803-1853) who used it to determine the speed of galaxies. First published in: Über das farbige Licht der Doppelsterne und einiger anderer Gestirne des Himmels, *Abh.königl.böhm.Ges.Wiss.* **2**, 465-482, 1843.

roughly consists of small diode laser (λ = 633 nm, probe depth ~100 μm[36]) and two scanning mirrors by which the laser beam can be made to scan over a rectangular area. The maximum size of the investigated area is 100 by 100 millimetres with a resolution of 64×64 points. Since the beam is halted for 50 ms at each point while measuring, a full-size scan takes almost 4 minutes. Most often a smaller, yet sufficiently large, area of interest was chosen. Since the calibration of the instrument is difficult (site dependent, blood concentration dependent) and no "golden standard" for measuring blood flows in capillaries exist, it is not possible to make absolute measurements with this kind of instrument in tissue. Nevertheless, it is possible to make comparative measurements and measure changes in perfusion quite well. The result is displayed as pseudo-colours images with red and blue denoting high and low perfusion, respectively. The data can then be statistically analyzed in the supplemented software (LDISOFT, 1.0, Lisca Development AB, Linköping, Sweden).

Chapter 3

Modelling light distribution in tissue

In the field of biomedical optics, light distribution is usually modelled within three conceptually different theoretical frameworks: Maxwell's equations, radiative transport and diffusion theory, c.f. Fig. 11.
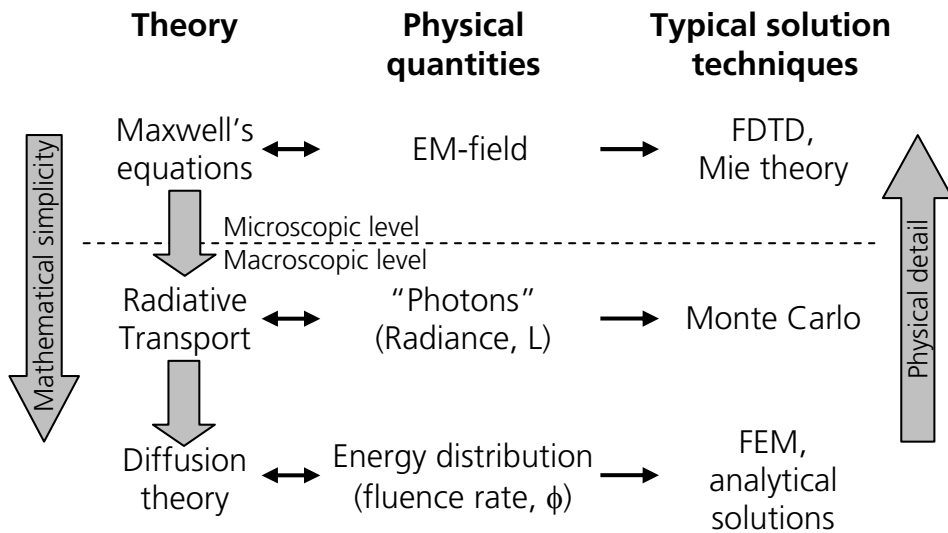
Fig. 11. Overview of different approaches to describe light propagation in tissue, (modified from Forster[37]).

Due to the complexity of Maxwell's equations their use within the field of biomedical optics has been limited; nevertheless they deserve being mentioned for completeness, c.f. 3.1. The theory behind radiative transport is further described in Sect. 3.2. Diffusion theory, which is derived from the radiative transport theory, is described in further detail in Sect. 3.3, while the applications are described in detail in Sect. 6.2.

All of the methods above rely on *a priori* knowledge of the optical properties. The vast research field of correctly determining the optical properties of tissue is, however, not further explored in this thesis, but I refer to e.g. Swartling[28] for the interested reader.

3.1 Electromagnetic theory

Using Maxwell's equations is the most fundamental way to describe the propagation of light in the context of classical physics. Here, light is viewed as an electro-magnetic field, interacting with the dielectric properties of the medium in which it propagates. There are only few analytical solutions to electro-dynamic problems. In the field of biomedical optics the most important example is the Mie theory[38,39], describing the scattering of an infinite plane wave by a small sphere. For more complex geometries approximate or numerical techniques have to be employed, such as the Rytov approximation[40] or the finite-difference time-domain method (FDTD)[41-43], or T-matrix theory [44-47].

3.2 Radiative transport theory

The radiative transport equation (RTE) can be derived from Maxwell's equations for highly idealized cases. We refer to the classical work of Chandrasekhar[48], Case and Zweifel[49] or Ishimaru[50] for a more detailed description. Below a brief outline of the concept is presented.

In transport theory the light is considered to be a collection of independently moving classical particles - photons – who do not interact with each other. In the framework of the RTE only the intensity of the light is considered, interference effects are not included in the model. A more heuristic approach to the RTE is based on a continuity equation for the photon density per solid angle, $N(\mathbf{r},\mathbf{s},t)$ [1/m^{3}sr]. This is the number of photons at the position $\mathbf{r}$ in with velocity v in the direction $\mathbf{s}$ at the time t. The radiance $L(\mathbf{r},\mathbf{s},t)$ [W/m^{2}sr]

$$L(\mathbf{r},\mathbf{s},t) = N(\mathbf{r},\mathbf{s},t) \cdot \frac{h v}{\lambda} \cdot c, \tag{10}$$

is then the light intensity per unit area and solid angle, h is Plank's constant and c the speed of light.

The time dependent RTE can be heuristically derived a by looking at the change of $N(\mathbf{r},\mathbf{s},t)$ in a closed volume element (Fig. 12) in the direction of $\mathbf{s}$[49]. The RTE can be expressed in terms of the radiance, utilizing Eq. (10)[51]:

$$\frac{1}{v}\frac{\partial L(\mathbf{r},\mathbf{s},t)}{\partial t} = \underbrace{-\mathbf{s}\cdot\nabla L(\mathbf{r},\mathbf{s},t)}_{a} - \underbrace{(\mu_a + \mu_s)L(\mathbf{r},\mathbf{s},t)}_{b} +$$

$$+\underbrace{\mu_s \int_{4\pi} L(\mathbf{r},\mathbf{s}',t)p(\mathbf{s},\mathbf{s}')d\omega'}_{c} + \underbrace{Q(\mathbf{r},\mathbf{s},t)}_{d} \quad , \tag{11}$$

The different terms on the right hand side in the RTE can be interpreted as
  a)   flow through the boundaries
  b)   absorption and scattering *off* the direction of **s**
  c)   scattering *into* the direction of **s**
  d)   sources, $Q(\mathbf{r},\mathbf{s},t)$ [W/m^{3}sr], located within the volume element.

The absorption and scattering coefficients (μ_a and μ_s) were introduced in Sect. 2.2, as the inverse mean free path length either between the light source and the absorption point, or between two consecutive scattering events, respectively. The phase function $p(\mathbf{s},\mathbf{s}')$ is the angular probability distribution of the scattering event, c.f. Sect. 2.2.3. There is no general analytical solution to the RTE in 3D, except for a few highly idealized cases[49].
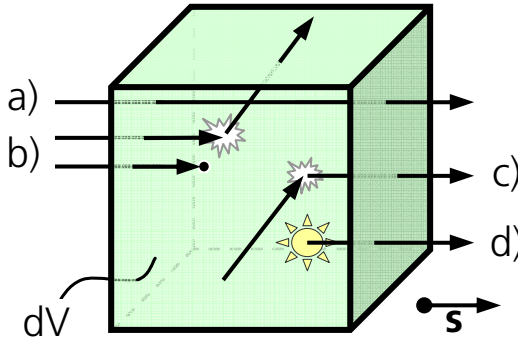
Fig. 12. Illustration of the terms included in the RTE: a) radiance b) absorption and scattering losses, c) gain by scattering, d) sources within dV. All terms are related to the direction of a unity vector s.

3.2.1   Analytical solution to for a thin slab

By applying the RTE to a thin slab geometry, illuminated by a collimated beam and using small solid-angle detection aligned along the optical axis an analytical solution can be obtained. In this case "thin" means that the thickness, d, of the slab is smaller than the inverse scattering coefficient, $1/\mu_s$. That implies that the probability of a single scattered photon being scattered back into the optical axis, by additional

scattering events, is very low. Therefore term c) in the RTE can be neglected. For the steady-state case, with no sources in the medium, this yields:

$$\mathbf{s} \cdot \nabla L(\mathbf{r}, \mathbf{s}) - \left(\mu_a + \mu_s\right) L(\mathbf{r}, \mathbf{s}) = \frac{\partial L(z)}{\partial s_z} - \left(\mu_a + \mu_s\right) L(z) = 0, \tag{12}$$

where the reduction to one dimension is motivated by the fact that the detection takes place along the optical axis. The solution to Eq. (12) can be written

$$L(z) = L_0 e^{-(\mu_a + \mu_s)z} = L_0 e^{-\mu_t z}. \tag{13}$$

This equation is also known as the generalized Beer-Lambert's law; see Fig. 13. The total attenuation coefficient μ_t is defined as $\mu_a + \mu_s$.
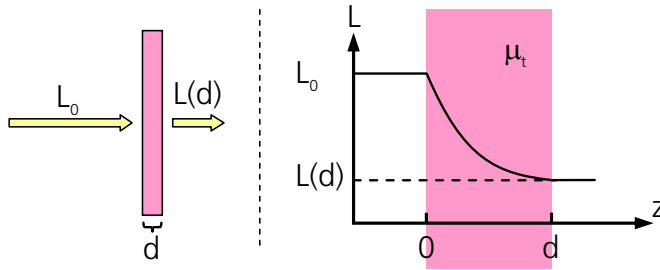
Fig. 13. Collimated beam incident in a thin slab geometry with thickness d (left). The radiance along the beam path is shown to the right.

3.2.2 Solution using Monte Carlo simulation

Monte Carlo simulation is a statistical method used to calculate the radiance distribution L($\mathbf{r}$,$\mathbf{s}$,t) by solving the RTE in a scattering medium. The method owes its name to the famous casino since it relies on the generation of random numbers in its calculations. By tracing a large number of photons a distribution of the light inside the medium is simulated. The simulation is based on three possible processes, namely that photons can be scattered, absorbed or exit the medium. The greatest advantage of this method is that any geometry, such as layered structures, inhomogeneities and any optical properties can be modelled. The main disadvantage is that each simulation might take quite long time, depending on the desired statistics of the results. Also, since the result is not analytical, any change of the input parameters requires a new simulation. The standard code for performing Monte Carlo simulations is the open source, public-domain, software package provided by Wang and Jacques[52,53]. In its original version it treats the light distribution in multiple layers of media and has therefore been labelled MCML - Monte Carlo modelling in Multi-Layered tissue.

In short, the method starts off by injecting a photon package with the initial weight W_0 into the medium. After a distance s the photon package is assumed to interact with the medium. A fraction ΔW of the package weight is then thought to be deposited at that point, after which a new direction for the photon package is simulated. All this is repeated until the photon package is absorbed or leaves the medium.

In more detail, the distance s is simulated as:

$$s = \frac{\ln(\zeta)}{\mu_t}, \tag{14}$$

with ζ being a random number between 0 and 1. By choosing s in this way it statistically follows Beer-Lambert's law [cf. Eq. (13)]. The deposited fraction of the photon weight after k steps, ΔW(k), is simply:

$$\Delta W(k) = W(k-1)\frac{\mu_a}{\mu_t}, \tag{15}$$

where W(k-1) is the incoming package weight. The scattering is also calculated through a random process. The scattering angle is determined according to the scattering phase function while the azimuthal angle is uniformly distributed ($\varphi = 2\pi\zeta$). The method is not formally restricted to using the Henyey-Greenstein phase function (replacing cos θ with ζ), but rather any suitable phase function can, in principle, be used.

To avoid having to simulate many small packages with minuscule weights, a trick is applied – the termination roulette. When a package reaches a certain minimum weight it is either completely terminated with a chance of 1/*m* to survive. If it survives, the weight of the package is increased *m* times so as to conserve the total energy.

3.3   Diffusion theory

There are no pure analytical solutions for relevant biomedical problems in the framework of electromagnetic or transport theory, and numerical solutions require long computational times. Under certain assumptions the RTE can be reduced to a diffusion-type equation, which is mathematically less complex. For some of these cases an analytical solution exists, in any case the numerical solutions are calculated much faster. For tissue optics, the diffusion theory is reviewed in more detail by e.g. Star[51].

3.3.1 Deriving the diffusion equation

The traditional approach when simplifying the RTE into the diffusion equation is to expand the radiance, L, in Eq. (11) into spherical harmonics, Y_{lm} and truncate the expansion.

$$L(\mathbf{r},\mathbf{s},t) = \sum_{l=0}^{\infty} \sum_{m=-l}^{l} \sqrt{\frac{2l+1}{4\pi}} L_{lm}(\mathbf{r},t) Y_{lm}(\mathbf{s})$$

$$\approx \frac{1}{4\pi} \big(\phi(\mathbf{r},t) + 3\mathbf{F}(\mathbf{r},t) \cdot \mathbf{s} \big) \quad , \quad (16)$$

The interpretation of Eq. (16) is that the radiance has been divided into an isotropic term (ϕ) and one term describing the angular dependence (**F**) of the radiance, while higher order terms were neglected. The expansion truncated after the N+1:th term is called the P_n-approximation. This is then called the P_1-approximation. The first two expansion coefficients can be calculated using

$$\phi(\mathbf{r},t) = \int_{4\pi} L(\mathbf{r},\mathbf{s},t)\,d\omega , \quad (17)$$

$$\mathbf{F}(\mathbf{r},t) = \int_{4\pi} L(\mathbf{r},\mathbf{s},t)\,\mathbf{s}\,d\omega . \quad (18)$$

The fluence rate, $\phi(\mathbf{r},t)$ [W/m^2], (the first expansion coefficient) is the light intensity per unit area at position **r** at a given time t; see Fig. 14. In contrast to the radiance, L, the fluence rate has no directional dependence; rather it is the total light intensity flowing in all directions at position **r**.
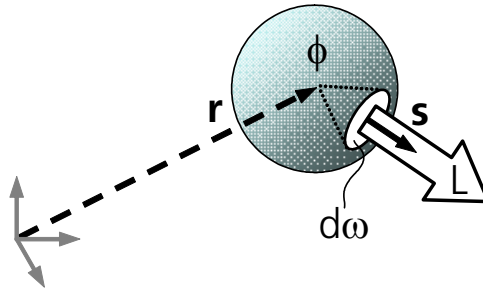
Fig. 14. Illustration of the relation between fluence rate ϕ(r,t) and radiance L(r,s,t). The fluence rate ϕ(r,t) at a given point r is the sum of the radiance over of an infinitesimal sphere.

For an isotropic light source, the photon flux is given by Fick's law as:

$$\mathbf{F}(\mathbf{r},t) = -D\nabla\phi, \tag{19}$$

with the diffusion coefficient D [m] defined as

$$D = \frac{1}{3(\mu_a + \mu_s')}. \tag{20}$$

The phase function p(cos θ) can be similarly expanded in a series of Legendre polynomials, P_l:

$$
\begin{aligned}
p(\cos\theta) &= \frac{1}{4\pi}\sum_{l=0}^{L}(2l+1)b_l P_l(\cos\theta) \\
&\approx \frac{1}{4\pi}(1+3g\cos\theta),
\end{aligned}
\tag{21}
$$

If the Henyey-Greenstein phase function (Eq. (6), p. 12) is expanded in Legendre polynomial, the expansion coefficients b_n are given by $b_n = g^n$. Although this function does not exactly represent the true scattering phase function in tissue for values of g smaller than 1 the higher terms become negligible and the truncation becomes a good approximation.

Finally, the source terms is expanded and truncated in a similar manner:

$$Q(\mathbf{r},\mathbf{s},t) \approx \frac{1}{4\pi}(q_0(\mathbf{r},t) + 3\mathbf{q}_1(\mathbf{r},t)\cdot\mathbf{s}), \tag{22}$$

Which for an isotropic source ($\mathbf{q}_1 = 0$) can be rewritten as:

$$Q(\mathbf{r},\mathbf{s},t) \approx \frac{1}{4\pi}q_0(\mathbf{r},t). \tag{23}$$

By inserting Eqs. (6), (16), (19), (21), and (23) into Eq. (11) this will yield the so called *time-dependent diffusion equation*:

$$\frac{1}{v}\frac{\partial\phi(\mathbf{r},t)}{\partial t} - \nabla(D\nabla\phi(\mathbf{r},t)) + \mu_a\phi(\mathbf{r},t) = q_0(\mathbf{r},t), \tag{24}$$

with $q_0(r,t)$ being the source term expressed in units of W/m^3. The steady-state solution to Eq. (24) for a homogenous medium (D constant) can then be simplified as:

$$-D\nabla^2\phi(\mathbf{r})+\mu_a\phi(\mathbf{r})=q_0(\mathbf{r}).$$
(25)

This is the *time-independent diffusion equation*, which will be referred to as the diffusion equation (DE) for the remainder of this thesis, since only steady-state processes will be considered.

3.3.2 Analytical solutions to the diffusion equation

Below the analytical solution to the DE (Eq. (25)) will be presented for two idealized cases: isotropic point source in an infinite medium and collimated beam incident on semi-infinite medium, see Fig. 15. The solutions to these model cases serve as good starting points in the understanding how light behaves in more complex geometries. Here, the term "infinite" refers to that no light escapes along the boundary of that surface and that the intensity at the boundary therefore can be set equal to zero.

a)   b)
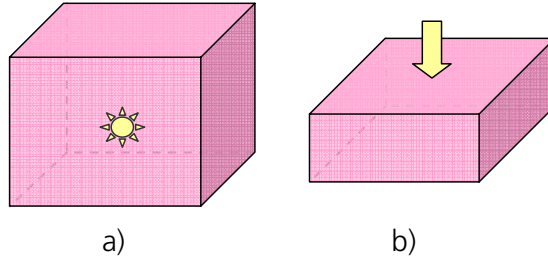
Fig. 15. Two general cases for which there is an analytical solution to the DE: thin slab, infinite medium, and semi-infinite medium.

Case a) Isotropic point source, infinite homogeneous medium

The diffuse fluence rate $\phi(r)$ at a distance r from an isotropic point source in an infinite medium can be written[51]:

$$\phi(r)=\frac{P_0\mu_{eff}^2}{4\pi\mu_a r}e^{-\mu_{eff}r},$$
(26)

where P_0 is the power [W] of the source and $\mu_{eff}=\sqrt{3\mu_a(\mu_a+\mu_s(1-g))}$ [m^{-1}] is called the effective attenuation coefficient, since it determines the attenuation of the light at long distances.

Case b) Collimated beam, semi-infinite medium

The case of a collimated beam incident on a semi-infinite diffuse medium is interesting since it can be though to mimic a narrow laser beam incident on a tissue surface. Similar to Case a) the source can be thought of as an isotropic point source at a depth of $1/\mu_s'$; see Fig. 16. To meet the boundary conditions at the surface a negative image of the source is introduced at $z = -(2z_e+z_0)$. At a virtual surface ($z = -z_e$) between the sources the flux will then be zero. The position of the virtual surface is $z_e \approx 2D$[50] if the refractive indices are matched at the interface or $z_e \approx 5.5D$ for a tissue-air interface ($n_{tissue} \approx 1.4$)[54]
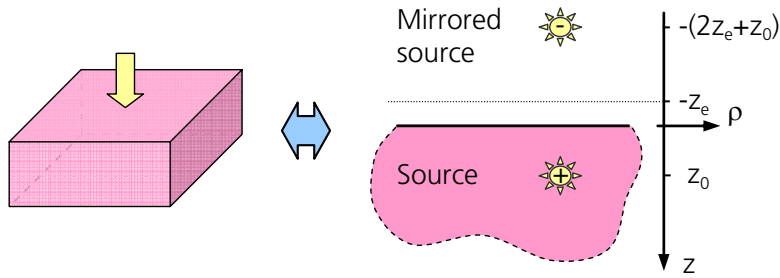
Fig. 16. A collimated beam incident on an semi-infinite medium can be modelled as an isotropic point source at a depth of $z_0 = 1/\mu_s'$. To ascertain correct boundary conditions at the surface a negative point source is also introduced, mirrored about a virtual surface at $-z_e$.

The steady-state fluence rate can now be expressed as[51]:

$$\phi(\rho,z) = \frac{P_0\mu_{eff}^2}{4\pi\mu_a}\left(\frac{e^{-\mu_{eff}\sqrt{(z-z_0)^2+\rho^2}}}{\sqrt{(z-z_0)^2+\rho^2}} - \frac{e^{-\mu_{eff}\sqrt{(z+z_0+2z_e)^2+\rho^2}}}{\sqrt{(z+z_0+2z_e)^2+\rho^2}} \right), \qquad (27)$$

with ρ being the horizontal coordinate. The reflectance R at the surface is

$$R(\rho) = \frac{1}{4\pi}\left(z_0\left(\mu_{eff}+\frac{1}{r_+}\right)\frac{e^{-\mu_{eff}r_+}}{r_+} - \left(z_0+2z_e\right)\left(\mu_{eff}+\frac{1}{r_-}\right)\frac{e^{-\mu_{eff}r_-}}{r_-} \right), \qquad (28)$$

with $r_+ = \sqrt{z_0^2+\rho^2}$ and $r_- = \sqrt{(z_0+2z_e)^2+\rho^2}$.

3.3.3 Numerical solutions to the diffusion equation

For the systems presented in Papers VI and VII (cf. Chapter 6) the light flux from optical fibres inserted in the tumours was calculated using Eq. (26) with a minor modification. The light emitted by each fibre will statistically be scattered by the tissue for the first time at a depth corresponding to $z = 1/\mu_s$ with a deflection angle determined by the scattering anisotropy g. This is equivalent to assuming that at a distance of $1/\mu_s'$ in front of the distal end of the fibre tip there will be an isotropically scattering point source[55,56], c.f. Fig. 17. The total light distribution from multiple fibres and more complex geometries was solved numerically using FEMLAB[©57], a commercial package for finite element method (FEM) calculations. In short, this method can provide numerical solutions of the light distribution in an arbitrary geometry. The volume (or area) of interest is descretized using a variable mesh, whose step size determines the accuracy of the solution. By defining both the relevant optical properties and the boundary conditions in the region of interest, point–wise solutions in the nodes of the mesh can be calculated. Doing this in three dimensions generally requires quite some computational time.
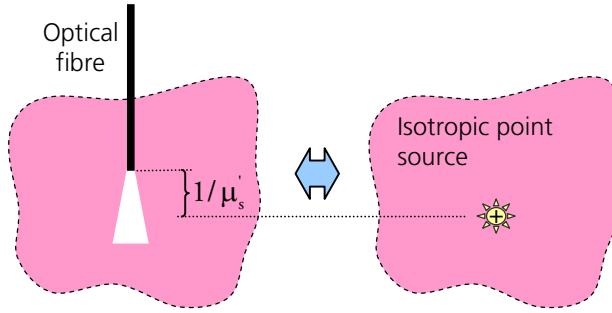
Fig. 17. An optical fibre inserted in an infinite medium can be approximated as an isotropic point source at a distance of $1/\mu_s'$ in front of the distal end of the fibre.

3.3.4 Limitations of the validity of the diffusion equation

When deriving the DE we made a series expansions of each quantity in Eq. (11) and neglected higher order terms. In doing so, mathematical simplicity was gained while losing accuracy of the mathematical solution with respect to the true light distribution. Also in the derivation of the DE we assumed that the light propagates diffusely, i.e. almost isotropically. An anisotropic source can be regarded as being (almost) isotropic at a distance of $1/\mu_s'$ from the source. This implies that the DE is not valid close to real sources. In order for the light to efficiently travel a distance of $1/\mu_s'$ the absorption in the medium has to be much smaller than the reduced

scattering or expressed differently; for the DE to be valid the following must apply: $\mu_a << \mu_s'$.

Furthermore, for the semi-infinite medium an artificial mirrored source can be introduced to meet the proper boundary conditions. For a slab geometry the source (and the mirrored source of case b.) would have had to be mirrored on both sides of the slab. Then the mirrored sources would in turn have to be mirrored and so on. This would in result in a series expansion with terms similar to those in Eq. (27). The thinner the slab, the more terms of the expansion have to be included for a correct result of the fluence rate. In addition to this, a change of the refractive index for the upper medium will alter the amount of internal reflection at the surface. This will result in an altered condition for the location of the mirrored source[56]. This illustrates the difficulties in finding accurate solutions close to boundaries.

Chapter 4

Fluorescence spectroscopy in medicine

This chapter deals with fluorescence spectroscopy focusing on the various applications developed with the field of medicine. The endogenous fluorescence, or *autofluorescence*, and fluorescence spectroscopy with tumour targeting compounds and the underlying physiological mechanisms are presented. Also the development of equipment and aspects on the evaluation of fluorescence data is discussed.

4.1   Historical background

The phenomenon of fluorescence (cf. Sect. 2.2) was first observed by Sir George G. Stokes[iv] in the mid 19th century when he observed that the mineral fluorite emitted visible light when illuminated by UV radiation[58]. Later, in 1911 Stübel observed the same phenomenon when illuminating animal tissue with UV light[59]. The fluorescence was then observed by the naked eye and was only characterized by its "reddish" colour. In 1924 this red florescence was observed in animal tumours and it was assumed to originate from various endogenous proteins[60]. Only much later it was confirmed that the main constituents responsible for tissue fluorescence were collagen, elastin, tryptophan[61], reduced nicotinamide adenine dinucleotide (NADH)[62,63] and flavins[64]. Since the composition of these constituents will be altered for several types of pathological conditions this will yield a change of the fluorescence spectrum and thus a potential for a diagnostic tool emerges. With the development of exogenous fluorescent tumour markers, e.g. HpD (1970's), and later ALA (1980's), the evolution of fluorescence spectroscopy within medicine quickly developed[65-70]. Most of these exogenous tumour markers, or *photosensitizers*, are not only used for fluorescence diagnosis but also for PDT (c.f. Chapter 6),

---

[iv] (1819-1903), British physicist and mathematician. Professor of Mathematics at Cambridge University in 1849. Also well-known for his contributions within vector analysis and studies of viscous flows (Navier-Stokes equations).

which certainly has contributed to the attractiveness of the modality. With the invention of the laser[v], a light source well suited for coupling into optical fibres has widely extended the possible clinical indications to include also endoscopical investigations. Fluorescence investigations utilizing laser excitation is frequently called laser-induced fluorescence (LIF).

4.2   Clinical context and prospects

In many clinical situations the patients are first visually examined, maybe even under illumination of a certain lamp[71,72], to find suspicious areas for further examinations. If there are several possible diagnoses, often a biopsy is collected, either randomly or according to a scheme. A small tissue sample is then excised and sent for histological examination, which normally takes a few days. The main competitive advantages of a fluorescence examination to this are:

−   non-invasive sampling, enabling an arbitrary number of measurements to be performed even on locations where multiples biopsies are unwanted or even impossible to perform
−   real-time results enabling an interactive procedure.

Since the penetration of visible light is very shallow compared to x-rays, fluorescence measurements are only possible to perform on superficial lesions (e.g. non-melanoma skin lesion; Papers I-III) or lesions accessible through endoscopes or invasive examinations (e.g. brain[73], urinary bladder[74], lung[75], colon[76], cervix[77,78]; Papers III, VIII-X). The shallow probing depth may not necessarily be a disadvantage. Since many malignancies start as changes in the epithelial layers, an increased probing depth would then result in higher influence of the deeply lying healthy tissue, thus reducing the sensitivity of the method.

In a first step the fluorescence measurement may serve as guidance for the traditional biopsies. The second step would be to draw diagnostic conclusions based on the fluorescence measurements, i.e. to perform an *optical biopsy*. Furthermore, if this also can be combined into an imaging modality that can visualize small lesions the method certainly has good clinical prospects. The working order to reach this stage is to carefully examine diagnosed tissue samples and analyze the features of the fluorescence spectrum. Subsequently, by selecting a number of interesting wavelengths for discrimination between the different tissue types, on-line fluorescence imaging of lesions is possible.

---

[v] Theodore H. Maiman, (1927-). American physicist. In 1960 he accomplished laser action in a ruby crystal, λ = 694 nm.

4.3 Autofluorescence

The spectrum of the endogenous fluorescence, or *autofluorescence*, of tissue when illuminated by UV or blue light is normally a smooth peak without sharp distinguishable features. The autofluorescence is made up by the individual fluorescence of a few constituents, referred to as *fluorophores*, which will be further described below. Data on the individual fluorescent properties can be found in Table 1. Due to the IC (cf. Fig. 4) some of the energy of the excitation light will be lost, resulting in a shift of the fluorescence towards longer wavelengths (lower energy). So, the excitation wavelength will partly determine the shape of a recorded fluorescence spectrum. For excitation at 337 nm and 405 nm, the maximum intensity of the autofluorescence of skin is located at approximately 410 nm and 490 nm, respectively; see Fig. 18 a). The amount of blood in the measured tissue greatly influences the spectrum in two ways. Firstly, it absorbs the excitation light reducing the over-all level of the fluorescence signal. Secondly, the different absorption of haemoglobin at different wavelengths (c.f. Fig. 6) may distort the fluorescence spectrum, leading to peaks or dips in the fluorescence spectrum, originating from the reabsorption of the fluorescence, rather than from the fluorescence properties themselves.

The fluorescence spectrum from selected fluorophores can be seen in Fig. 18 b). Also, the excitation and emission properties of some fluorophores can be found in Table 1, below. The absolute position of the fluorescence peak for the individual fluorophore might be slightly shifted when measured *in vivo*.
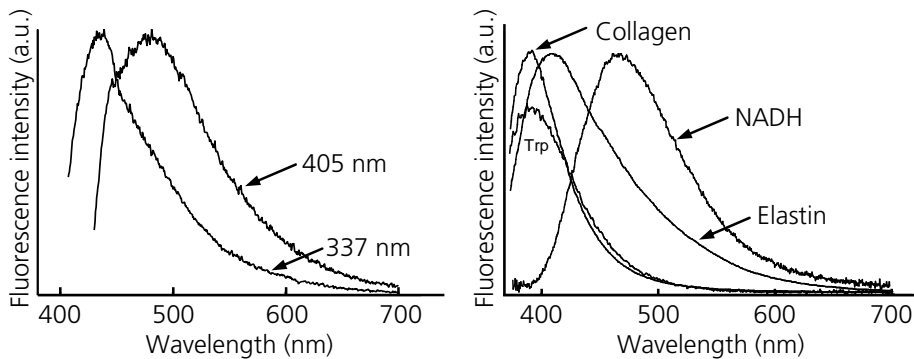
Fig. 18. a) The autofluorescence of healthy skin when excited at 337 nm and 405 nm, respectively, recorded with the system described in Sect. 4.5.1. b) The fluorescence from individual fluorophores when excited at 337 nm[79]; other peaks may dominate when excited at other wavelengths.

Fluorophore	Excitation wavelength (nm)	Emission wavelength (nm)
Collagen	270; **340** 285	**395** 310
Elastin	260; 360 425 **460**	410 490 **520**
NADH	350	460
Endogenous porphyrins	400-405	580; 630 (CoP) 630; 690 (Hp) 635; 705 (Pp)
Tryptophan	**275** 337	**350** 390

Table 1. Major excitation wavelengths and corresponding emission maxima for different endogenous fluorophores[80-82], with bold typeface indicating the strongest fluorescence intensity. The exact position of these peaks varies depending on if measured *in vivo* or *in vitro* (depending also on the solvent used). CoP: coproporphyrin, Hp: haematoporphyrin, Pp: protoporphyrin.

4.3.1 Collagen and elastin

The proteins collagen and elastin are the two main constituents in the extra-cellular connective matrix. As the name implies the connective matrix is responsible for connecting, anchoring and supporting the various structures of the body. The rope–like collagen exists in various forms, each denoted by its Roman numeral. Collagen I is the most abundant form (90 % of total collagen) and can be found in skin, ligaments, bone, dentin and internal organs[83]. Collagen IV is also interesting since it is found in the basal layers of epithelial tissue. The rubber band like elastin gives the elastic properties to tissue such as skin, blood vessels, etc. These proteins dominate the autofluorescence when excited at about 340 nm.

4.3.2 NADH/NAD$^+$

NADH and its oxidized counterpart NAD$^+$ are vitamin B$_3$ co-enzymes serving as hydrogen carriers in several stages of the metabolism i.e. the citric acid cycle[vi] and the oxidative phosphorylation[2] inside the mitochondria. Since many malignancies have an increased metabolic rate this will increase the level of the NAD$^+$ while reducing the level of available NADH. In addition, the pH is often slightly lower in malignant tissue than in healthy tissue pushing the redox balance between NADH and NAD$^+$ towards NAD^{+}[84]. These two effects and the fact that NADH is highly fluorescent while NAD$^+$ is not (when excited above 300 nm) is believed to explain the widely reported lower blue-green autofluorescence of malignant and pre-malignant tissue[85-87], Paper I.

4.3.3 Other fluorophores

The main fluorophores of tissue are described above although a few other fluorophores deserve being mentioned. The essential amino acid tryptophan also exhibits fluorescence (at 350 nm) especially when illuminated at 275 nm. Flavins (FAD, FMN) constitute another source of fluorescence that will emit yellow-green light (500-600 nm)[88] when excited at 480 nm. Fluorescence from endogenous porphyrins (e.g. haematoporphyrin, protoporphyrin, coproporphyrin) is sometimes observed in cancerous or pre-cancerous lesions[89,90] (or in warts, unpublished data by author). Ghadially et al.[91] showed that this fluorescence is due to bacterial activity in necrotic areas of the lesion. When excited at about 405 nm each of theses endogenous porphyrins emit fluorescence at two typical peaks, somewhere between 580 and 705 nm, depending on the type of porphyrin[80,82,90].

4.4   Fluorescent tumour markers

As mentioned previously, the development of fluorescence diagnostics has been closely connected to the evolution of PDT, mainly due to the fact that many of the tumour markers also fluoresce. Thus, a lesion can be both diagnosed and treated at the same occasion with the same drug. If used only for diagnostics, the drug dose given is often several magnitudes lower than the corresponding therapeutic dose to minimize unwanted photosensitization. Attempts have also been made to develop tumour markers without the photosensitizing effect, e.g. caroteneporhyrins[92,93] and chlorin derivatives[94]. The therapeutic part will be further described in Chapter 5. Table 2 on page 46 contains a listing of some commercially available tumour

---

[vi] Also known as the *Krebs cycle* named after the German-born British biochemist Hans A. Krebs (1900-1981) who discovered most of the step in the cycle. K. was awarded the Nobel Prize in Physiology or Medicine in 1953.

markers also used for PDT. In this thesis the focus will be on ALA and its successors, which will therefore be presented further below.

4.4.1 ALA and its esterified derivatives

ALA is currently one off the most popular photosensitizer and fluorescence tumour marker precursors. It is an endogenous amino acid, which in itself is not fluorescent or photochemically active at all. ALA takes part in the *haem cycle*; c.f. Figure 19; a biochemical, irreversible process taking place partly in the mitochondria and partly in the cytosol of all living cells, ultimately producing haem. Depending on the type of lesion examined, ALA can be administered, e.g. intravenously, orally, topically (mixing it in a cream for skin lesions) or be instilled (in the urinary bladder).
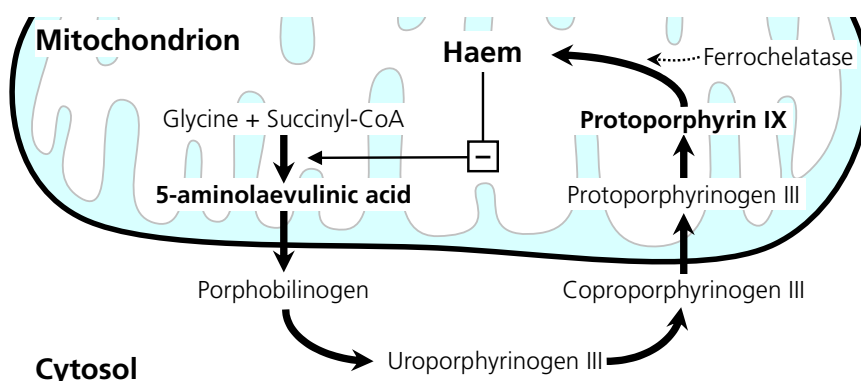
Figure 19. Outline of the haem cycle. By external administration of aminolaevulinic acid (ALA) it is possible to bypass the negative feedback (dashed line) of haem, thereby increasing the rate of the whole cycle. The relatively slow synthesis of haem from protoporphyrin IX (PpIX), catalyzed by the enzyme ferrochelatase (dotted line), will eventually lead to build-up of PpIX, which may then be used for fluorescence investigations and/or PDT.

The first steps in the process are relatively fast compared to the very last, step where haem is synthesized by incorporating an Fe^{2+}-ion in the centre of the porphyrin ring of PpIX; a process catalyzed by the enzyme ferrochelatase; Figure 20. Haem, in turn exhibits a negative feedback on the enzymatic step leading to ALA synthesis. By administering excess amounts of ALA it is possible to bypass this negative feed-back and increase the activity of the following steps of the haem cycle. All of the above will in time lead to an accumulation of PpIX, a substance that is both fluorescent and can be used for PDT, c.f. Chapter 5. When excited at about 405 nm PpIX will fluoresce, mainly at 635 nm but also at 705 nm. The maximum levels of fluorescence are reached after approximately 4 to 6 hours after topical admin-istration and the PpIX is fully cleared within 48 hours. When used for PDT the

PpIX will be consumed during the therapeutic irradiation forming several chlorin-type photoproducts, mostly photoprotoporphyrin, which in turn exhibit a broad, albeit weaker, fluorescence at about 670 nm (Fig. 24, p. 41).
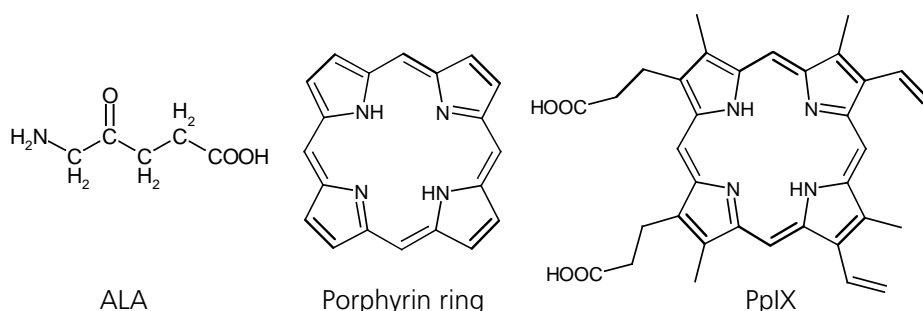
Figure 20. The chemical structure of ALA, the porphyrin core, and PpIX. PpIX differs from haem in that it lacks a Fe^{2+}-ion in the centre of the porphyrin ring.

The tumour localising effect of ALA-induced PpIX is well documented[95,96], although the exact explanation to this is still somewhat debated. Some of the theories raised are as follows. Firstly, proliferating cells (mostly found in tumours but also inflammations) are often found to have an increased haem cycle activity as compared to normal cells[97-99]. Secondly, malignant cells have been found to have a lowered activity of ferrochelatase[97,98,100-102]. Thirdly, in skin the keratin layer of healthy skin is fairly impermeable to ALA[103], while this layer is usually damaged for several conditions, allowing the ALA to penetrate more easily into lesions. A fourth explanation could be that the lower pH in tumours results in a higher PpIX production. Finally, tumours may have less readily accessible iron needed in the conversion of PpIX to haem. These are all suggested factors that, depending on the type of lesion, may influence the uptake of ALA, production of PpIX and subsequent conversion to haem.

For skin lesions, such as BCC and carcinoma *in situ*, efforts have been put in to overcome the limited penetration of ALA by, e.g., mechanically stripping the upper layer of the skin, *stratum corneum* (SC)[104,105] or by iontophoretic ALA delivery[106]. Other ideas concern the use of esterified ALA derivatives, e.g. ALA-ME, in which a hydrogen atom of the carboxyl group (COOH), of ALA is replaced by a longer ester chain in the form $(CH_2)_xH$, thereby increasing the lipophilicity of the ALA compound[107-109]. The higher lipophilicity will facilitate the diffusion of ALA through the skin, although a too high lipophilicity will result in the ALA derivative getting accumulated in the SC instead. Before entering the haem cycle the esterified ALA types are enzymatically converted to ALA resulting in an identical synthesis, from that point on, for both types of ALA[110,111].

In Papers I-VII the fluorescence from PpIX, induced by ALA and ALA-ME, was monitored in connection to PDT. In Papers I-III human BCCs were examined, where the ALA or ALA-ME was administered by mixing the sensitizer prodrug in a lotion to a weight concentration of 20%, 4-6 hours prior to therapeutic irradiation. For the experimental tumours examined in Papers VI-VII, 13 Wistar/Furth rats weighing approximately 250 g, with adenocarcinomas inoculated on each hind leg were administered ALA intraperitoneally at a dose of 100 mg/g body weight, one hour prior to irradiation.

4.5   Instrumentation and detection principles

Fluorescence measurements are in principle fairly straight-forward and the equipment can be made quite simple. By filtering away the reflected excitation light it is possible to obtain quite strong signals, virtually in real-time, of tissues[vii]. The problems arise when it comes to the interpretation of the fluorescence signal, for several reasons. As shown previously, the fluorescence peaks are mostly broad and several fluorophores may overlap. The different optical properties at the excitation and detection wavelengths also influence the signal. For excitation light in the UV region the penetration depth is only a few hundred microns while the visible fluorescence may very well travel a couple of millimetres, while being filtered by the tissue itself. A consequence of this is that the intensity of a fluorescence signal cannot be directly interpreted as a corresponding fluorophore concentration. Another consequence is that the measurement set-up, both on the excitation and detection side, strongly influences not only the signal level but also the spectral shape of the detected signal; c.f. Fig. 21[112]. Notably, in Fig. 21.b) the detection fibre shields the excitation light from reaching the tissue below the detection fibre, mostly quenching the fluorescence in the blue-green region (<500 nm) while having less influence on the yellow-red light (>580 nm). To monitor the overall performance of the system a stable fluorescence reference should be employed (in our case, 10 mg Rhodamine 6G dissolved in 60 ml ethylene glycol). Furthermore, the spectral response of the detection system should be compensated for using for example the emission of a calibrated black-body radiator.

It is also possible to measure not only the spectral characteristics of the fluorescence spectrum, but also the temporal aspects of the spectrum can be investigated. Several imaging fluorescence systems have been developed[113-115]. Such systems fall beyond the extent of this thesis and are only mentioned here as a reference. The fluorescence systems, being point monitoring (Papers I, III, V–VII, and VIII) and

---

[vii] The chlorophyll in plants can also be remotely monitored using LIF.

imaging (Papers IX-X) systems, utilized in the work presented within the framework of this thesis are briefly described below.
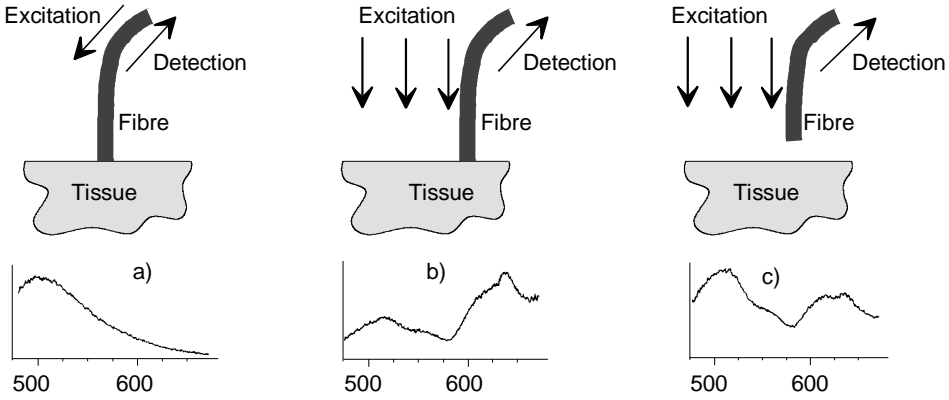
Fig. 21. Illustration of the influence of the measurement set-up to the detected fluorescence signal, from Eker[112].

4.5.1 Point monitoring systems

Point measurements from are illustrated in Fig. 21. Here the detected signal is dispersed in wavelength to yield a full emission spectrum at each single point. In most cases set-up a) will be the most convenient using the same fibre both for excitation and detection. The thin optical fibre can easily be inserted in an endoscope or even in the lumen of a needle making it possible to measure on almost any organ. In a clinical setting care must be taken to ascertain that proper antiseptic or sterile conditions are maintained.

Two different point monitoring systems developed by our group were used during the measurements, Papers I, III-V, VIII. The first system[116] utilizes a pulsed nitrogen laser (λ = 337 nm, W_{pulse} = 75 μJ, t_{pulse} = 3 ns, prf = 15 Hz) for either direct measurements or to pump a dye laser (λ = 405 nm, W_{pulse} $\approx$ 1 μJ, dye: diphenylstilbene in dioxane). The wavelengths of this system are then appropriate for both autofluorescence and porphyrin fluorescence investigations, respectively. The wavelength used is controlled by the software, which in turn controls the hardware. It takes less than 1 second to change between the wavelengths. By utilizing pulsed excitation and gated (intensified), detection this system is insensitive to the ambient light, which can be quite strong, e.g., in an operating theatre. Generally, the spectra from 20 laser pulses are recorded and accumulated to increase the S/N-ratio. One measurement (using both wavelengths) then takes approximately 3 seconds. The system is quite compact, the optical unit measures 47×40×21 cm^3 and weighs 19 kg.

The recent development of diode lasers with wavelengths extending into the blue–UV region have made them very attractive as sources for even more compact fluorosensors. One such system has been developed[117,118] and extensively evaluated by our group; bench-marked against the system described above. The system consists of fairly few basic components, c.f. Fig. 22. A diode laser (λ = 396 nm, W = 1.2 mW) driven by a 9V standard battery is focused into a 600-μm fibre via a dichroic beam-splitter. The distal end of the fibre is held in gentle contact to the sample. The induced fluorescence is collected by the same fibre and guided back into the spectrometer, this time passing the beam-splitter and a filter (to remove the elastically scattered light).
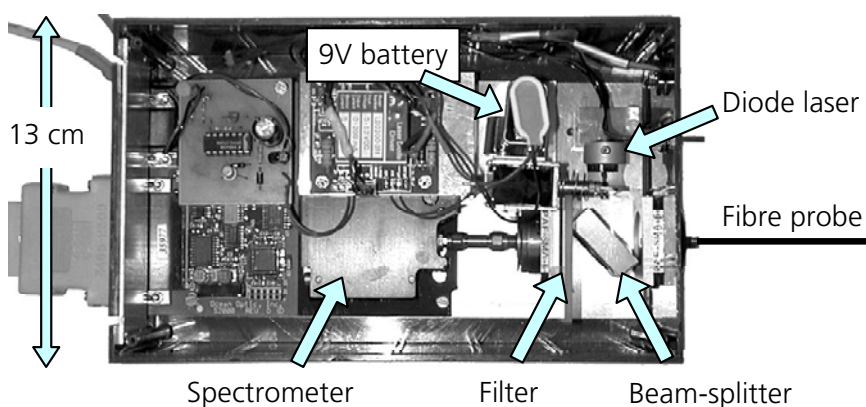
Fig. 22. Top view of the diode fluorosensor.

This system does not utilise pulsed laser excitation and gated detection. Thus, the ambient light will interfere with the measurements, although this can be compensated for by first acquiring a background. This is done by first measuring on the sample with the laser turned on and then immediately measuring for an equal mount of time with the laser turned off.

This diode laser-based system proved to have comparable performance as the nitrogen laser based-system for investigations in connection to ALA-PDT. However, for autofluorescence measurements shorter wavelengths should be employed (~340 nm) but at the point of assembly that kind of lasers were not commercially available. A fluorosensor based on diode lasers was later incorporated in the system presented in Sect. 6.1.

4.5.2 Imaging systems

The strength of a point monitoring system is the ability to acquire a full spectrum of the sample in virtually no time with fairly simple and cheap equipment. The big disadvantages of these systems, when it comes to clinical applications, is that small lesions are difficult to find and that the fluorescence information cannot easily be interpreted as pertaining to a certain illness. The purpose of imaging systems is mainly to facilitate the clinicians in finding lesions that may be difficult, or even impossible, to find by the naked eye, and then use traditional methods to diagnose the suspicious areas. Attempts to develop imaging systems with built-in interpretation of the fluorescence are being pursued, one of which is briefly presented below. A recent review on imaging fluorescence systems can be found in reference [119].

Single/multi colour imaging systems

With *a priori* knowledge of the wavelength dependence of the lesions being investigated, it is possible to limit the number of wavelengths measured. One such system was developed in Lund (now intellectual property of Xillix Technologies Corp, BC, Canada), employing multi-colour real-time fluorescence imaging adopted for detection of porphyrin fluorescence[115,120,121]. The fluorescence is generated by a pulsed frequency doubled Alexandrite laser (tuned to λ = 390 nm). The detection system consists of an optical set-up that disperses three wavelength bands on separate areas of a CCD detector while at the same time acquiring a video image of the area being investigated. In principle, a false colour image is then generated by forming a dimensionless contrast function, F_K, based on the intensities in the three wavelength bands:

$$F_K = \frac{Red - k_1 \cdot Green}{k_2 \cdot Blue} .$$

(29)

Here Blue, Green, and Red are the intensities in the regions: 420–480 nm (~tissue autofluorescence), 480-580 nm (reference region), and 580-750 nm (~porphyrin fluorescence), respectively. The constants k_1 and k_2 have different values for different applications. This will result in a high value of F_K for areas with high fluorescence intensity in the red region i.e. regions with high porphyrin contents. By superimposing the contrast function over the video image it is possible to display a live image of tissue sensitized with porphyrins.
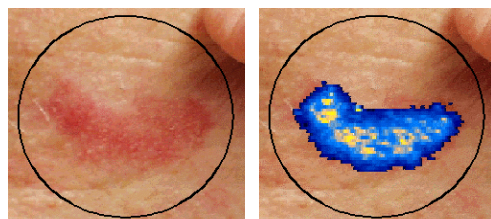
Figure 23. A recorded image of a BCC acquired with the multi-colour system developed in Lund, without (left) and with (right) the superimposed contrast function.

In this a category of systems also a commercially available endoscope (developed by Karl Storz GmbH & Co. KG, Tüttlingen, Germany) is worth mentioning, since it is widely used at many clinics. Basically, it consists of a filtered Xenon arc lamp (λ = 375-440 nm) inducing the fluorescence and an imaging CCD camera with a high-pass filter (λ > 450 nm) for detection. Due to the small wavelength difference between the excitation light and the detection filter some of the elastically scattered light is allowed to reach the detector along with the fluorescence. These two light components are then displayed on a monitor, where areas with high porphyrin contents will stand out as brighter than areas with low porphyrin contents. Using a foot switch the clinician then chooses between the fluorescence imaging mode or the normal endoscopic view. This system has been used extensively for detection of tumours in the urinary bladder[122,123] but also for tumours in the oral cavity[124,125], breast tumours[126], cervical[127], and gastrointestinal[128] lesions.

Multispectral imaging systems

An instrument extracting the spectral information in many wavelengths bands for cervical malignancies is being built and developed by Science and Technology International®, Honolulu, USA. The HSDI® system (Hyper-Spectral Diagnostic Imaging) combines a conventional video colposcope with a line-scanning push-broom, multi-spectral imaging system. The cervix is being illuminated line by line and the re-emitted light is collected by an imaging CCD detector (typical resolution: 150×150 pixels), after being dispersed by a spectrometer (λ = 400-760 nm). For each pixel in the illuminated line the spectrum will be perpendicularly positioned, with respect to the extent of the line. By then scanning the illumination light over the cervix a spectrum is acquired for every pixel of the whole cervix. This can be done in both fluorescence and white-light illumination mode and each measurement takes approximately 12 and 7 seconds, respectively. The ambition with such a complex system is not only to assist the clinician in finding possible lesions, but also to accurately delineate and diagnose lesions. Papers VIII-X regard data collected on 111 patients in a larger clinical study performed in Vilnius, Lithuania, where our point monitoring system (described in the previous section) served as fluorescence reference to the HSDI® system.

Another system extracting full spectral information in each spatial position is the SpectraCube® system[129,130] (Applied Spectral Imaging, Ltd., Migdal Ha'Emek, Israel). In this system the area being examined is imaged through a Sagnac-interferometer, capturing the interferogram of the examined area. The interferogram is then Fourier-transformed yielding the spectrum of each pixel. Instead of a scanning in the spatial domain (like in the HSDI® system), the scanning is now performed in the spectral domain.

4.6   Data analysis of fluorescence spectra

Since the fluorescence emission spectrum of tissue normally does not exhibit any sharp, distinct features the information of a large part or the whole spectrum needs to be evaluated. Even if the penetration of the excitation light is fairly limited the fluorescence signal (which is shifted towards the red part of the spectrum) can travel a distance in the order of a few millimetres. The probing depth may then span over both diseased and healthy tissue limiting the diagnostic value of the fluorescence signal. The most obvious fluorescence indication of a tissue dysfunction is the lowered intensity in the blue green part of the spectrum (450-510 nm, c.f. Fig. 24) but this is not specific for malignancies, also benign conditions and inflammations may yield a similar decrease in signal. Furthermore, both the inter patient and intra patient variations are considerable, emphasizing the need of acquiring a spectrum from healthy tissue from a region close to the lesion. The above illustrates some of the difficulties in the interpretation of autofluorescence data. Still, successful attempts to do so have been performed by various groups on different tissue types: colon[76,131], cervix uteri[132], atherosclerotic plaque[133,134].
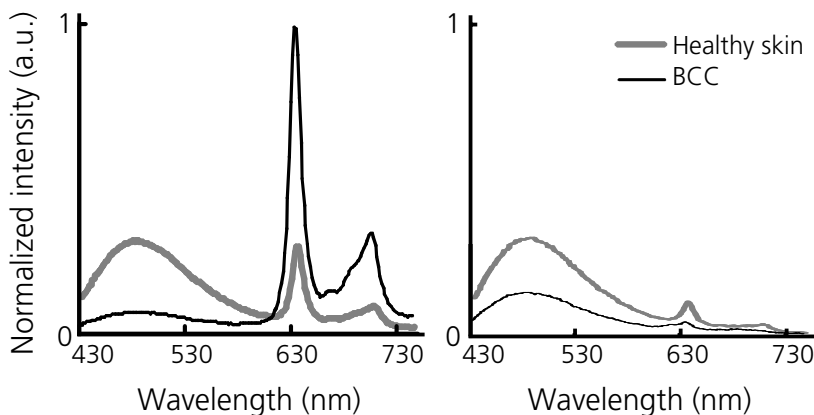

Fig. 24. Typical fluorescence spectra (λ_{exc} = 405 nm) from a BCC and adjacent healthy skin in connection with PDT: a) 6h after ALA application b) after the therapeutic irradiation.

Fluorescence spectroscopy using an exogenous fluorophore greatly simplifies the data analysis. The spectral information used can be reduced down to the region/s where the fluorophore has its highest influence. In Paper I, the fluorescence from BCCs sensitized with ALA and ALA-ME was studied in order to assess possible differences in PpIX concentration following administration of the two sensitizers. This could be of interest for photodynamic therapy. The fluorescence build-up was monitored during the treatment for both the lesion and the surrounding healthy skin. The fluorescence data was quantified by forming the ratio between the intensity at the PpIX fluorescence peak (635 nm) in relation to the maximum intensity for the autofluorescence (480-490 nm). We found this ratio to be significantly higher for ALA-ME treated lesions while at the same time being slightly lower for the healthy skin, compared to ALA. This suggests that ALA-ME is superior to ALA in that a lower light dose could be delivered for photodynamic therapy with preserved therapeutic effect. Also the data suggested that illumination after 4h, instead of the clinical praxis of 6h (for ALA), could be employed in order to avoid excessive build-up of PpIX in the healthy skin.

Again the evaluation was conducted by forming a ratio, similar to the case of the imaging system. Forming ratios is a very simple albeit powerful technique to qualitatively evaluate fluorescence spectra. Many unknown factors influencing the fluorescence spectrum cancels out by forming the ratio, i.e. fluctuations of the excitation source and detection efficiency, variations in the incident illumination angle. There is no direct relation between the concentration of a fluorophore and the fluorescence intensity because of the different optical properties at the excitation and the emission wavelength. Still, a method to asses the concentration from fluorescence data has been presented by Sterenborg *et al.*[135], who used two excitation wavelengths and two detection wavelengths.

Chapter 5

Photodynamic therapy

Photodynamic therapy, or PDT, is a modality for treatment of various localised lesions, mostly malignant or pre-malignant tumours, using therapeutic light and a photosensitizer in the presence of tissue oxygen. Following administration, the photosensitizer (or its pre-cursor) will accumulate to a higher degree in diseased cells than in healthy cells. After allowing the sensitizer to build-up for a certain amount of time (typically a few hours), the whole lesional area is illuminated by therapeutic light. By matching the wavelength of the therapeutic light to the absorption of the sensitizer, much of the light will be absorbed by the photosensitizer, which will induce a chemical reaction resulting in the formation of oxidative species[136].
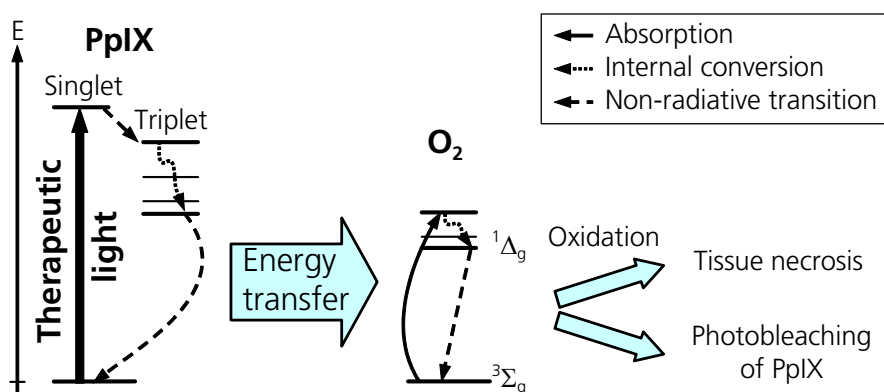
Fig. 25. A schematic view of the physical mechanism behind ALA-PDT. Following irradiation of the therapeutic light the sensitizer (here PpIX) is transferred to one of its metastable triplet states. The sensitizer may then give its excess energy to a neighbouring oxygen molecule, thereby forming singlet oxygen [$0_2(^1\Delta_g)$]. This highly reactive oxygen will a) induce tissue necrosis and b) degrade the photosensitizer, resulting in a photobleaching of the PpIX.

The modality has several benefits as compared to conventional tumour treatment, e.g. chemotherapy, ionising radiation or surgery:

- Selective treatment: during treatment the healthy tissue will be spared due the low concentration of the photosensitizer in these cells making this modality an attractive option when treating lesions in the vicinity of sensitive healthy structures. Also, PDT usually results in a good cosmetic outcome since the healthy connective tissue most often is left intact.
- Light as radiation source: will not induce malignancies as ionising radiation might do. The treatment can be repeated many times since there is no life-time dose limitation as with radiotherapy (the connective tissue is left intact).
- Polyclinical treatment: the total treatment takes approximately 4-6 hours, under supervision of personnel for less than 1 hour.
- Self regulating treatment: the sensitizers are consumed during the treatment, effectively reducing the risk of over-treating a lesion.
- Relaxed sterility conditions: the treatment itself is frequently minimally invasive.

The main disadvantages are mainly the limited penetration depth of both the treatment light and the sensitizer (for topical applications). This reduces the clinical indication to comprise superficial and non-pigmented lesions. Unfortunately, malignant melanomas are responding well following PDT. To a varying degree the patients also experience a certain discomfort, often described as a "stinging", "prickling" or "burning" sensation, even though the temperature of the lesion only increases a few centigrades during irradiation[137], Paper II. Local anaesthesia can be administered, although spraying the treatment area with cool water greatly reduces the sensation. Finally, some sensitizers have a very long clearance time making the patients sensitive to light for several days or weeks.

Clinical PDT has been explored for more than 20 years and the modality is gradually achieving clinical acceptance. Today PDT can be considered as an option for many indications. Many photosensitizers have been approved and further clinical trials are in progress. Lights sources that were once complex and expensive are now being replaced by compact, cheap light sources. All of the above are reasons why PDT is attracting both clinical and commercial interest. Two excellent reviews on the clinical use of PDT can be found in Morton *et al.*[138] and Brown *et al.*[139].

5.1 The physiological mechanisms behind PDT

Following the irradiation by the treatment light, the sensitizer may react with its microenvironment in two principally different, competing ways:

- Type I reaction – in which the sensitizer transfers its energy to a neighbouring atom or molecule, forming a free radical.
- Type II reaction – in which the sensitizer reacts with the molecular oxygen in tissue, transforming harmless triplet oxygen $[O_2(^3\Sigma_g)]$ into highly oxidative singlet oxygen $[O_2(^1\Delta_g)]$.

The type II process is believed to be the dominant process in PDT. These highly toxic compounds have been estimated to diffuse 0.01-0.02 µm before reacting with their closest surrounding - the malignant cells – causing a primary tissue necrosis, c.f. Fig. 25. In the absence of oxygen, the type I reaction dominates but the cells have protective mechanisms that can handle most free radical formation much more efficient than singlet oxygen formation[140]. Excess oxygen is therefore a prerequisite for an efficient PDT effect.

Due to the very short diffusion range of the singlet oxygen (~1/10 the size of a red blood cell), the sub cellular location of the sensitizer is important for the cell killing effect. Suggested sub cellular targets are lysosomes and membranes inducing a combination of necrosis and apoptosis, respectively[141,142]. These are also the primary PDT effects contributing to the cell death as observed clinically. In particular, for intravenously administered sensitizers the high levels of sensitizer in the circulating blood plasma will target the membranes of the endothelial cells, resulting in a considerable primary vascular damage. The secondary effects are due to the membrane damage that partly stimulates a release of inflammatory and immuno-stimulating mediators that further induces apoptosis[143], and partly impairs the circulation, the latter is believed to be especially lethal for proliferating cells, such as malignant cells[144].

The PDT process is efficiently self-terminating for many kinds of sensitizers. The photosensitizer acts as catalyst in the excitation processes described above, returning to its original state after the energy transfer. The produced singlet oxygen (or free radicals) may though counteract irreversibly with the photosensitizer, oxidising it. The process is called photobleaching, since the amount of available sensitizer will be greatly reduced, efficiently stopping the PDT process. The therapeutic result is that the lesions, up to a certain point, cannot be over treated.

5.2   Photosensitizers

The first photosensitizer used was HpD and much research has been performed on understanding the PDT mechanisms and improving the properties of photosensitizers since. There are several properties to take into account when comparing photosensitizers. Since the penetration of light in tissue is wavelength dependent and increases towards the red part of the spectrum it is desirable to have a sensitizer with a high absorbance as far as possible into the red region to be able to treat thicker lesions. Today there are many sensitizers absorbing at longer wavelengths than the initial 630 nm corresponding to HpD. Also it is important to have a high tumour targeting selectivity or that the sensitizer targets structures that are more sensitive in tumours than in healthy tissue, e.g. the vascular bed. Also the timescale by which the sensitizer both accumulates and leaves the body is of great patient interest. Unfortunately, some sensitizers have a very long-lasting photosensitizing effect, for some sensitizers lasting several months. Other aspects to take into account could be the administration route and the possible side-effects of the sensitizer itself. The following section presents a selection of sensitizers considered as possible candidates for superficial and interstitial-PDT, c.f. Table 2.

Sensitizer	Commercial name	λ_{exc} (nm)	Approved clinical indications*
HpD	Photofrin®	630	lung, oesophagus, cervix uteri, urinary bladder, gastric cancer
ALA,	**	635	actinic keratosis
ALA-ME	Metvix®		actinic keratosis, BCC
mTHPC	Foscan®	652	head, neck cancer,
BPD	Verteporfin, Visudyne®	690	AMD***

Table 2. Commercially available photosensitizers for oncological indications, which may also be used for fluorescence investigations. *Not all indications in Europe are approved in the USA and vice versa. **generic substance *** Age-related Macular Degeneration, not an oncological indication, but widely employed.

5.2.1 Porphyrins

The porphyrin PpIX, and its pre-cursor ALA, were described in detail in Sect. 4.4.1. The successful use of porphyrins for PDT was first explored by Diamond *et al.* in 1972, who tested haematoporphyrin on cell cultures[145]. This was soon followed up

in several clinical studies[146,147] were HpD was used as sensitizer. However, patients administered with HpD remain sensitive to light for several weeks and the sensitizing compound is quickly degraded upon light exposure. Since the biochemical processes of porphyrins in the body have been known for long, the idea to use ALA as a sensitizer precursor emerged and was experimentally tested by Malik and Lugaci[148] and Peng et al.[149] in 1987, quickly followed by the first clinical studies by Kennedy and Pottier[103,150] in 1990 and 1992. Work with ALA-PDT also started early in the Lund group[151].

The pioneering work using with HpD has paved the way for the development of the clinical protocols and handling of safety issues regarding PDT, as well as illustrating the benefits and disadvantages of the modality. HpD is now approved for a number of indications and it proven to be efficient in eradicating tumours, easy to administer (intravenously), and also it has a low general toxicity. The disadvantages are mainly the low selectivity[144] with a ratio of 2-3:1 in concentration (tumour to healthy tissue), the long build-up time (~48-72 hours) and the slow clearance time (~2-6 weeks). These are issues that many of the subsequent compounds have been aiming to improve.

5.2.2 Chlorins

Chlorins are chemically similar to porphyrins, differing only in that one, or more, of the double bonds in the porphyrin ring are reduced for the corresponding chlorin. One of the implications of this is that the absorption spectrum of chlorins is shifted towards longer wavelengths, compared to porphyrins, giving chlorins a green colour while porphyrins usually are red. One well known chlorin is the chlorophyll of green plants in which a Mg^{2+}–ion has been incorporated in the core of the molecule. Normally plants have a very efficient conversion of the sunlight into chemically available energy, strongly quenching the emission of fluorescence. Even so plants can be made to fluoresce by overloading that conversion with a strong excitation light, yielding the typical double peak fluorescence (c.f. Fig. 24) at about 685 nm and 740 nm[152].

A clinically[153-155] used chlorin for PDT is meta-tetrahydroxyphenylchlorin (mTHPC) also know as Temoporfin or under the commercial name: Foscan®. It was clinically approved 2001 for palliative head and neck cancer. It has shown to be highly efficient ($\lambda = 652$ nm) even at low drug doses, like HpD, it suffers from low selectivity, slow build-up (96 h, typically) and long clearance time (3-6 weeks).

Another sensitizer belonging to the chlorin family is, despite the name, benzoporphyrin derivative (BPD) or Verteporfin. It has been successfully used for treatment of age related macular degeneration (AMD)[156,157]. AMD is a disease in which vascular generation on the *choroidea* eventually will lead to blindness in elderly patients. The clinical ease of this method, for both clinician and patient, has

highly contributed to it popularity. After 10 minutes of intravenous infusion, followed by 15 minutes of build-up, the patient is irradiated for 83 seconds (λ = 690 nm, ϕ = 600 mW/cm^2, dose: 50 J/cm^2), efficiently closing the leaky vessels sparing the overlying retinal tissue.

5.3 Oxygen

Readily available oxygen, provided by the hemoglobin in the blood vessels, is a fundamental element in PDT. In order to ascertain that sufficient oxygen is available during the PDT process, two aspects of the treatment have to be considered. Firstly, there could be a transient depletion of the available oxygen as a direct result of the treatment. Some groups have suggested that by delivering the light in fractions, the oxygenation (and maybe also the sensitizer level) is allowed to recover, resulting in a more efficient treatment[158-162], although this effect is not always present[162,163]. This leads up to the second consideration; since sensitizers may target the vascular bed of the lesion (or the surrounding healthy tissue) it is possible that this might permanently impair the oxygen supply to the lesion. This is somewhat supported by the fact that a too large initial illumination does not lead to a significantly increased tissue damage, as a short initial illumination might[162].

In an equipment developed within the framework of this thesis, the therapeutic light is delivered in sessions of 30-60 seconds followed by a measurement session (with the therapeutic light shut off) lasting approximately 45 seconds (c.f. Sect.6.1). This is repeated until reaching the full treatment time. With our system it is not possible to determine if the oxygen level recuperates during the short period of time the treatment light is shut off, Paper VII. What we do see is that the oxygen level decreases steadily during the whole treatment, suggesting that a longer dark interval would be required to restore the oxygen level. It still remains to be investigated if this has any effect on the treatment efficacy.

5.4 Light

5.4.1 Light sources

A frequently used light source for clinical PDT has been high-power tungsten lamps. These light sources have a broad spectral distribution making a large part of the emitted light ineffective for the excitation of the photosensitizer since the absorption spectra of these compounds generally are relatively narrow-banded. Although there seems to be synergistic effects of a mild hyperthermia in connection to PDT[164], large amounts of heat needed to be filtered out with that kind of lamps. Furthermore, these sources had a poor beam quality making them difficult to couple efficiently into optical fibres or endoscopes. With the introduction of high power diode lasers at the wavelengths used for PDT, a light source well adapted to

both the absorption spectrum of the photosensitizer was available, not generating much excess heat in the treatment area. The beam characteristics of most lasers also make them good candidates for coupling into optical fibres. The development of semi-conductor lasers have lead to cheaper, compact, turn-key laser systems at nearly any wavelength of the visible spectrum, with sufficiently high output even for the needs of PDT. Also for superficial treatment, the use of even cheaper light emitting diode arrays (LEDs)[165,166] may be used. Even if the output of an individual LED is quite low they can be combined into a matrix giving a sufficient total output.

A convenient way to compare the effectiveness of different light sources is by comparing the relative biological efficiency (RBE)[167,168]. The RBE is given by:

$$RBE = \frac{\int I(\lambda)E(\lambda)d\lambda}{\int I(\lambda)}, \tag{30}$$

where $E(\lambda)$ is the normalized action spectrum of the sensitizer and $I(\lambda)$ is the intensity of the lamp.

The light source used in Papers I–VI was a fibre-coupled diode laser (Ceralas™ PDT 635, Biolitec, Bonn, Germany) emitting light at 635 nm with a maximum power of 2W. The superficial lesions, in Papers I–II, were irradiated with a total surface energy of 60 J/cm^2 while the fluence rate did not exceed 150 mW/cm^2 so as to not induce any hyperthermal effects[164]. By having a microlens at the tip of the output fibre a uniform light distribution was achieved over the illuminated area. For Papers III to VI the same light source was coupled into a light distributor with six output fibres, each fibre giving between 100-180 mW out of a 600 µm clear-cut optical fibre. The light sources used in the system presented in Paper VII are described in Sect. 6.1.1.

Comment on the use of dosimetric units

Commonly there is an inconsistency between the terminology used by clinicians compared to the mathematical definitions. When clinicians refer to fluence rate (or dose rate) they refer to the incident intensity per unit *area* [W/m^2], which mathematically is equivalent to the irradiance. These quantities are identical only for light travelling in one direction, which is the case for the incoming light in superficial PDT. The quantities are not identical as soon as the light enters the body due to the scattering of the tissue.

The clinical dose is calculated as the clinical fluence rate multiplied by the treatment time, resulting in the *incident* energy per unit *area*. The common units used for the clinical fluence rate and dose are: mW/cm^2 and J/cm^2, respectively[viii]. On the other hand, the mathematical dose, $W(\mathbf{r})$ $[J/m^3]$ J/m^3 is defined as the *deposited* energy per unit *volume* according to:

$$W(\mathbf{r}) = \mu_a \int \phi(\mathbf{r}, t) dt \,, \tag{31}$$

[viii] For cylindrical diffusers the corresponding units are: mW/cm and J/cm.

Chapter 6

Interstitial Photodynamic Therapy

Interstitial PDT (IPDT) has emerged as a means of overcoming the limited penetration of the therapeutic light[169-171]. By delivering the light using multiple optical fibres inserted into a tumour, thick lesions and/or deeply lying lesions can be successfully treated with PDT[172]. Virtually any kind of lesion can be accessed in this way. Much of the work presented in this thesis was done in order to develop and evaluate equipment for IPDT, Papers III-VII. The idea behind the developed systems is to use the inserted fibres not only to deliver the therapeutic light but also to optically monitor parameters of relevant therapeutic interest in order to improve the clinical outcome, Fig. 26.
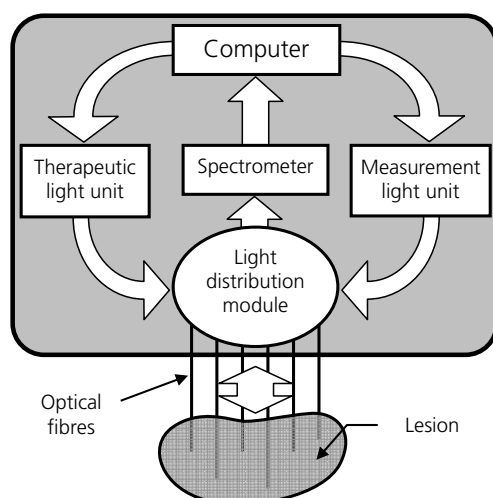

Fig. 26. Overview of the concept of the equipment developed. The optical fibres inserted in the lesion are used both for therapeutic irradiation and measurement of treatment parameters. The feed-back from the measurements should then be used to interactively control the therapy. Figure from Paper VII.

These measurements will probe the tissue between the fibres and a low-resolution tomographic image could be calculated. Since PDT relies on the simultaneous presence of light, sensitizer, and oxygen; those were the parameters we aimed to retrieve. For the first system (IPDT-I) developed in this work, described in Paper VI and used in Papers III-V, only the intensity of the light at the therapeutic wavelength could be measured. In its successor (IPDT-II) we believe that we can accurately assess all three parameters, c.f. Paper VII. Below both systems are presented briefly, the focus will mostly be on the second generation system. Also results from initial clinical experiences will be discussed.

6.1 Overview of the system set-up

IPDT-I consisted of an external fibre-coupled, 2W diode laser (Ceralas™ PDT 635, Biolitec, Bonn, Germany) being coupled into the light distribution unit, distributing the incoming laser light into either 3 or 6 output optical fibres (core diameter: 400-μm, outer diameter: 0.9 mm) inserted in the lesion; see Fig. 27. The maximum therapeutic output with this system was 0.7 W. The laser light was distributed using a set-up consisting of lenses and beam splitters that allowed for a moveable photodiode to be positioned in the beam path of each individual fibre, c.f. Fig. 27 (right). These photodiodes where sequentially used to measure the collected light at the tip of every patient fibre during the treatment. A measurement session lasts for approximately one minute. The fluorescence measurements performed in connection to PDT were done using the point monitoring systems described in Sect. 4.5.1.
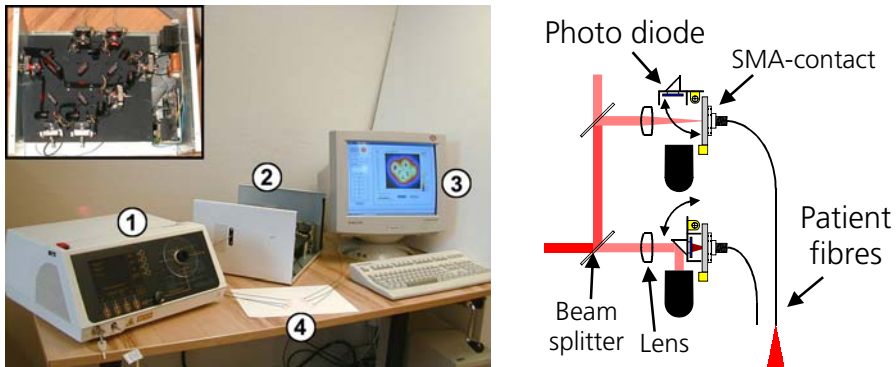
Fig. 27. Left: System overview (IPDT-I), from Paper III. 1) Treatment laser, 2) Light distribution unit, 3. Computer, 4. Treatment fibres. Inset left: top view of the light distribution unit. Right: Detail from the light distribution unit showing one patient fibres in treatment mode (top) and one fibre in detection mode with the photodiode measuring the light intensity at the fibre tip (bottom), from Paper VI.

Fig. 28. System overview of the IPDT-II from Paper VII (left) and in its present state (right).

In IPDT-II the treatment laser and the different components for measuring sensitizer fluorescence, oxygen levels and light distribution were combined into one single compact system; c.f. Fig. 28. The system measured $30\times43\times21$ cm^3 and weighed 12 kg (laptop not included). The therapeutic light was generated by six, 250 mW, pigtailed, diode lasers ($\lambda = 635$ nm) coupled into a light distribution unit, resulting in a maximum total therapeutic output, of 1.2 W, after losses in the beam-splitter unit. The module for measuring the photosensitizer fluorescence is based on the concept of the diode fluorosensor described in Sect. 4.5.1. The oxygen saturation level is assessed by monitoring the penetration of light at two separate wavelengths, similar to the concept of clinical pulse oximetry[173-175].

Both systems have been used only for ALA-PDT. For use with another sensitizer the therapeutic light source would have to be changed accordingly. This is trivial in the case of the IPDT-I but this was also incorporated when designing the IPDT-II. By changing the light module (consisting of both the therapeutic light sources and the dosimetric light sources) the system will work at any given wavelength with preserved performance.

6.1.1 *Therapeutic light measurements*

The experience with both systems (Papers III and VII) when measuring the penetration of the therapeutic light is that the penetration decreases during the treatment. This is an interesting finding since this would result in the need for a first order correction of the treatment time in order to really deliver the calculated amount of light to the entire tumour volume. This change in penetration has also been found to vary between patients supporting the concept of individual dosimetry.

A recently suggested[176] mechanism to the altered penetration at the particular wavelength, is that the oxygen consumed during PDT results in decrease of the level of HbO_2 in favour of the more absorbing Hb; c.f. Fig. 6. Another possible explanation could be that the decreased penetration may be due to damage to the tissue microcirculation. The actual reason for the mechanism still remains to be thoroughly examined.

6.1.2 Photosensitizer level

For fluorescence investigations of superficial lesions with ALA sensitization excitation at 405 nm is often used. We have found that monitoring the fluorescence at that wavelength can only be done prior to starting the therapeutic irradiation. Since the penetration depth of the light is very short at that wavelength, only the immediate tissue closest to the fibre tip will influence the fluorescence signal. At that position the fluence rate of therapeutic light will be at its highest level efficiently bleaching off all available sensitizer. In our initial measurements at this wavelength (unpublished), no sensitizer fluorescence could be detected after 30 seconds of therapeutic irradiation.

Since PpIX has two fluorescence peaks in the red region (635 and 705 nm) it is possible to excite the fluorescence at 635 nm and detect the emitted fluorescence at 705 nm. Light at these wavelengths will travel a sufficiently long distance inducing the fluorescence with light from one fibre and detecting it with another fibre, which is the approach taken in the IPDT-II system. We demonstrated that it was possible to monitor the sensitizer level and the typical PDT photobleaching with that setup.

The interpretation of the bleaching of the fluorescence signal cannot be easily correlated to the induced PDT damage and corresponding treatment outcome. Boere *et al.*[177] have recently presented experimental data that suggest that the initial photobleaching rate is correlated to a higher level of epithelial damage. This needs to be further investigated.

6.1.3 Oxygen saturation level

The tissue oxygen saturation level is given by:

$$S_{O_2} = \frac{[HbO_2]}{[Hb] + [HbO_2]},$$ (32)

was measured using a broad-band LED covering the wavelength interval of 750-800 nm. At the isobestic point at 797 nm (c.f. Sect. 2.2.1) the absorption of HbO_2 and Hb are equal, while at slightly shorter wavelengths Hb has a higher absorption. In principle, by forming the ratio between the light intensity at the isobestic point

(as a reference) and a shorter wavelength it is possible to monitor changes in the oxygen saturation level, assuming that the changes in light intensity are due to alterations in the blood oxygen supply. The reduction in oxygen saturation during IPDT was found to correlate well with the reduced penetration of the treatment light. This supports the hypothesis that the reduced penetration of the therapeutic light is indeed caused by an increase of Hb in favour of HbO_2, due to the PDT-induced oxygen consumption.

6.2 Software design and dosimetry considerations

Both systems are controlled by custom-made software. The program requires that the tumour geometry is entered, whereby the fibre positions are calculated in order to ascertain that the threshold light dose is delivered to the tumour boundary in the shortest time possible. With knowledge of the fibre positions the light dose is calculated by solving the DE, Eq. (25) using FEM simulations, c.f. Sect. 3.3.3. The source term $[q_o(r)]$ in Eq. (25) is now exchanged with a sum of sources $[\Sigma q_i(r_i)]$. For the IPDT−I the FEM calculations were done in a custom-made program written in C++. For the IPDT−II those calculations are performed using FEMLAB. The custom-made FEM program of the first system was developed in order to reduce the long computation times required by commercial FEM programs available at the point of assembly. For the IPDT−II, FEMLAB combined with faster computers give reasonable calculation times in the order a few minutes.

The light distribution in the tumour is calculated using diffusion theory, which will result in an erroneous calculated light distribution close to the fibre tips. This will still have limited importance for delivered therapeutic dose. Since the fibres are inserted into the tumour volume, the therapeutic light dose in the centre of tumour will always be very much higher than the value at the tumour boundary. Thus, even if the calculated values at the centre are wrong the tumour centre will receive (more than) enough therapeutic light. At the same time, the tumour boundary will dictate the required treatment time and in this region the diffusion equation will be a much better approximation.

There are many aspects that need to be considered in order to properly utilise the dosimetric measurement to correlate the data to the therapeutic result, some of which are illustrated by Wilson et al.[178]. Data from the first clinical treatments with the IPDT-II system is now being evaluated, and will be presented in a manuscript presently in preparation by Ann Johansson.

Acknowledgements

This work would not have been possible to perform without the support and encouragement of numerous people to whom I now wish to convey my warmest gratitude.

Stefan Andersson-Engels, my supervisor - for the dedication and guidance through the years and for always lending me an ear when things have gone bad. Thank you also for the summer school, the kayak excursions, floor ball matches, football games, and all other social events that makes the medical group such a pleasant place to work in.

Katarina Svanberg, my co-supervisor – and clinical mentor, for the heartily welcome into the medical world and the never-ending patience. Your professionalism and ability to always put the patient first has impressed me greatly. Thank you for making me part of so many interesting clinical situations and cultural events. I have really enjoyed working together with you.

Sune Svanberg, my other co-supervisor – if there had been a Nobel-prize in enthusiasm, I am sure you would have been awarded it. If, that is, you weren't chairing that committee too ... This combined with your humbleness and deep knowledge in all possible fields has made it a true privilege to work with you.

My former PhD-student colleagues – Lotta Eker, Sara Pålsson, Eva Samsøe, Maria Stenberg, Claes af Klinteberg, Niels Bendsøe, Thomas Johansson, Johannes Swartling, Ulf Gustavsso - as well as my present colleagues – Ann Johansson, Jenny Svensson, Nazila Yavari, Lotta Gustafsson, Christoffer Abrahamsson, and Tomas Svensson – all deserve my deepest gratitude. I can't even imagine how this work would have been like without you! A warm thank goes out to the exotic post-docs I've had the pleasure to get to know: Aruna Prakasa, Tuan Pham, Hua Zhao, and Florian Forster.

I would also like to thank all the persons I have had the privilege to work with in various trails – the colleagues in Riga, Latvia, in Vilnius, Lithuania, at STI in Honolulu, USA. Also Thomas Andersson and Kerstin Jakobsson are greatly acknowledged for their dedicated work at SpectraCure, hopefully transforming the concept of IPDT into a clinically available reality.

To all my friends –Växjö-gängen, BK Legolas, Gerda, Surfers - thank you for being there!

To Elin y *La Familia* – your love and support throughout the years have carried me through all this. I love you!

Summary of papers

Paper I reports on the diagnostic and therapeutic outcome when using topically applied ALA and ALA-ME for PDT of BCCs. Laser-induced fluorescence was used to measure the build-up of PpIX and, in addition to that, the superficial perfusion and temperature was imaged.

Paper II reports on clinical measurements that indirectly provide information on the vascular mechanisms during topical PDT. An infrared camera was used to measure the superficial temperature and the superficial perfusion was studied using a laser Doppler scanning instrument.

Paper III reports on a clinical trial where thick BCCs were treated with the equipment for IPDT presented in Paper VI.

Paper IV presents an experimental estimation of the photodynamic threshold dose on rodent hind legs muscle, inoculated with an adenocarcinoma cell line, sensitized with PpIX.

Paper V reports on initial results of the interstitial system for PDT

Paper VI presents the equipment developed for PDT (IPDT–I) with on-line dosimetry used in Papers III and V. This system can interactively asses the light distribution inside of the tumour.

Paper VII presents the successor to the system presented in Paper VI. In addition to the features of its predecessor, this system has a build-in fluorosensor and it also has the capability to monitor changes in oxygen saturation level during treatment.

Paper VIII deals with histopathological evaluation of cervical biopsies. The orientation, location and pathological variability within biopsies are recorded to allow correlation between the histopathological diagnosis and the fluorescence spectra.

Papers IX-X are connected with Paper VIII since they originate from the same clinical trial, where a fluorescence and reflectance imaging system was used for investigations of the cervix. The correlation between the fluorescence spectral shape and histopathological diagnosis is discussed in Paper IX. In Paper X, the spatial variation in the cervical images is calculated.

Contribution by the author to the papers

Paper I.   Major part of the clinical measurements, data evaluation, and manuscript preparation.

Paper II.   Substantial part of clinical measurements. Contributions to scientific discussion and manuscript preparation.

Paper III.   Major part of the clinical measurements, data evaluation, and manuscript preparation.

Paper IV.	Contributions to the experimental measurements and the scientific discussion.
Paper V.	Substantial part of the experimental measurements. Large part of data evaluation and manuscript preparation.
Paper VI.	Substantial part of the experimental measurements and the manuscript preparation. Contribution to the data evaluation.
Paper VII.	Substantial part of the equipment assembly, experimental measurements, data evaluation and manuscript preparation.
Paper VIII.	Substantial part of the fluorescence point monitoring and study design, contributions to the scientific discussion.
Paper IX.	Substantial part of the fluorescence point monitoring.
Paper X.	Participation in the clinical trail. Evaluation of point monitoring fluorescence spectra

References

1. Svanberg, S., *Atomic and Molecular Spectroscopy – Basic Aspects and Practical Applications*, 4th edition, (Springer Verlag, Heidelberg, Germany, 2003).

2. Vander, A., Sherman, J. and Luciano, D., *Human physiology - The mechanisms of body functions*, 7, (McGraw-Hill, New York, 1998).

3. Clarke, R.H., Isner, J.M., Gauthier, T., Nakagawa, K., Cerio, F., Hanlon, E., Gaffney, E., Rouse, E. and DeJesus, S., Spectroscopic characterization of cardiovascular tissue, *Lasers Surg. Med.* **8**, 45-59 (1988).

4. Alfano, R.R., Pradhan, A., Tang, G.C. and Wahl, S.J., Optical spectroscopic diagnosis of cancer and normal breast tissues, *J. Opt. Soc. Am. B* **6**, 1015-1023 (1989).

5. Caspers, P.J., Lucassen, G.W., Wolthuis, R., Bruining, H.A. and Puppels, G.J., In vitro and in vivo Raman spectroscopy of human skin, *Biospectroscopy* **4**, 31-39 (1998).

6. Jacques, S.L., Wang, L. and Hielscher, A.H., Time-resolved photon propagation in tissues, in *Optical-Thermal Response of Laser-Irradiated Tissue,* eds. Welch, A.J. and van Gemert, M.J.C., pp. 305-332 (Plenum Press, New York, 1995).

7. Boulnois, J.-L., Photophysical processes in recent medical laser developments: a review, *Lasers Med. Sci.* **1**, 47-66 (1986).

8. Hale, G.M. and Querry, M.R., Optical constants of water in the 200-nm to 200-μm wavelength region, *Appl. Opt.* **12**, 555-563 (1973).

9. Jacques, S.L. and McAuliffe, D.J., The melanosome: Threshold temperature for explosive vaporization and internal absorption coefficient during pulsed laser irradiation, *Photochem. Photobiol.* **53**, 769-775 (1991).

10. Prahl, S.A.. Tabulated molar extinction coefficient for hemoglobin in water. Oregon Medical Laser Center, 1998. omlc.ogi.edu/spectra/ hemoglobin/summary.html.

11. Spott, T., Characterization of layered tissue structures with diffusely propagating photon-density waves, Dissertation thesis, Norwegian University of Science and Technology, Department of Physical Electronics, Trondheim, Norway (1999).

12. Antonini, E. and Brunori, M., *Hemoglobin and myoglobin in their reactions with ligands*, 1, (North-Holland Publishing Company, Amsterdam, 1971).

13. Mines, A.H., *Respiratory Physiology*, 3, (Raven Press, New York, 1993).

14. Hecht, E., *Optics*, 2nd, (Addison-Wesley Publishing Company, Reading, Massachusetts, 1987).

15. Bolin, F.P., Preuss, L.E., Taylor, R.C. and Ference, R.J., Refractive index of some mammalian tissue using a fiber optic cladding method, *Appl. Opt.* **28**, 2297-2303 (1989).

16. Tearney, G.J., Brezinski, M.E., Southern, J.F., Bouma, B.E., Hee, M.R. and Fujimoto, J.G., Determination of the refractive index of highly scattering human tissue by optical coherence tomography, *Opt. Lett.* **20**, 2258-2260 (1995).

17. Star, W.M., Light dosimetry *in vivo*, *Phys. Med. Biol.* **42**, 763-787 (1997).

18. Mourant, J.R., Johnson, T.M., Doddi, V. and Freyer, J.P., Angular dependent light scattering from multicellular spheroids, *J. Biomedical Optics* **7**, 93-99 (2002).

19. Beauvoit, B., Evans, S.M., Jenkins, T.W., Miller, E.E. and Chance, B., Correlation between the light scattering and the mitochondrial content of normal tissues and transplantable rodent tumors, *Anal. Biochem.* **226**, 167-174 (1995).

20. Kitai, T., Beauvoit, B. and Chance, B., Optical determination of fatty change of the graft liver with near-infrared time-resolved spectroscopy, *Transplantation* **62**, 642-647 (1996).

21. Eker, C., Shah, N., Pham, T. and Tromberg, B., Non-invasive determination of blood, water, and fat content in human breast tissue using frequency-domain photon migration spectroscopy, Unpublished work (2000).

22. Beuthan, J., Minet, O., Helfmann, J., Herrig, M. and Müller, G., The spatial variation of the refractive index in biological cells, *Phys. Med. Biol.* **41**, 369-382 (1996).

23. af Klinteberg, C., On the use of light for the characterization and treatment of malignant tumours, Dissertation thesis, Lund Institute of Technology, Lund, Sweden (1999).

24. Jacques, S.L., Alter, C.A. and Prahl, S.A., Angular dependence of HeNe laser light scattering by human dermis, *Lasers Life Sci.* **1**, 309-333 (1987).

25. Arnfield, M.R., Tulip, J. and McPhee, M.S., Optical propagation in tissue with anisotropic scattering, *IEEE Trans. Biomed. Eng.* **35**, 372-381 (1988).

26. Yoon, G., Welch, A.J., Motamedi, M. and van Gemert, M.J.C., Development and application of three-dimensional light distribution model for laser irradiated tissue, *IEEE J. Quant. Electr.* **QE-23**, 1721-1733 (1987).

27. Cheong, W.-F., Prahl, S.A. and Welch, A.J., A review of the optical properties of biological tissues, *IEEE J. Quant. Electr.* **26**, 2166-2185 (1990).

28. Swartling, J., Biomedical and atmospheric applications of optical spectroscopy in scattering media, Dissertation thesis, Lund Institute of Technology, Lund, Sweden (2002).

29. Öberg, P.Å., Laser-Doppler flow-metry, *Crit. Rev. Biomed. Eng.* **18**, 125-163 (1990).

30. Salerud, E.G. and Öberg, P.Å., Single-fibre laser Doppler flowmetry. A method for deep tissue perfusion measurements, *Med. Biol. Eng. Comput.* **25**, 329-334 (1987).

31. Larsson, R., Öberg, P.Å. and Larsson, S.E., Changes of trapezius muscle blood flow and electromyography in chronic neck pain due to trapezius myalgia, *Pain* **79**, 45-50 (1999).

32. Löfgren, H., Larsson, R. and Larsson, S.E., Outcome of surgery for cervical radiculopathy evaluated by determination of trapezius muscle micro-circulation and electromyography, *Eur. J. Pain* **5**, 39-48 (2001).

33. Wang, I., Andersson-Engels, S., Nilsson, G.E., Wårdell, K. and Svanberg, K., Superficial blood flow following photodynamic therapy of malignant skin tumours measured by laser Doppler perfusion imaging, *Br. J. Dermatol.* **136**, 184-189 (1997).

34. Enejder, A.M.K., af Klinteberg, C., Wang, I., Andersson-Engels, S., Bendsoe, N., Svanberg, S. and Svanberg, K., Blood perfusion studies on basal cell carcinomas in con-

junction with photodynamic therapy and cryotherapy employing laser Doppler perfusion imaging, *Acta Derm. Venereol.* **80**, 19-23 (2000).

35. Wårdell, K. and Nilsson, G., Laser Doppler imaging of skin, in *Non-invasive methods and the skin,* eds. Serup, J. and Jemec, B.E., pp. 421-427 (CRC Press, Boca Raton, 1995).

36. Jakobsson, A. and Nilsson, G.E., Prediction of sampling depth and photon pathlength in laser Doppler flowmetry, *Med. Biol. Eng. Comput.* **31**, 301-307 (1993).

37. Forster, F.K., Modellierung der Lichtausbreitung in biologischem Gewebe unter Berücksichtigung der Mikrostruktur, Dissertation thesis, Fakultät für Naturwissenschaften der Unversität Ulm, Germany, (2004).

38. van de Hulst, H.C., *Light scattering by small particles*, (Wiley, New York, NY, 1957).

39. Bohren, C.F. and Huffman, D.R., *Absorption and scattering of light by small particles*, (John Wiley & Sons, Inc., New York, NY, 1983).

40. Jackson, J.D., *Classical Electro-dynamics*, (John Wiley & Sons, Inc., USA, 1975).

41. Gustafsson, B., Kreiss, H.-O. and Oliger, J., *Time-dependent problems and difference methods*, (John Wiley & Sons, New York, 1995).

42. Stott, J.J. and Boas, D.A., A practical comparison between time-domain and frequency-domain diffusive optical imaging systems, in *OSA Biomedical Topical Meetings, OSA Technical Digest*, Proc. Optical Society of America, Washington DC 626-628 (2002).

43. Finite-Difference Time-Domain Lite-rature Database. FDTD.org, 2004. www.fdtd.org.

44. Waterman, P.C., New formulation of acoustic scattering, *J. Acoust. Soc. Am.* **45**, 1417-1429 (1968).

45. Barber, P.W. and Yeh, C., Scattering of electromagnetic waves by arbitrarily shaped dielectric bodies, *Appl. Opt.* **14**, 2864-2872 (1975).

46. Hill, S.C., Hill, A.C. and Barber, P.W., Light scattering by size/shape distributions of soil particles and spheroids, *Appl. Opt.* **23**, 1025-1031 (1984).

47. Nilsson, A.M.K., Alsholm, P., Karlsson, A. and Andersson-Engels, S., *T*-matrix computations of light scattering by red blood cells, *Appl. Opt.* **37**, 2735-2748 (1998).

48. Chandrasekhar, S., *Radiative transfer*, (Oxford University Press, London, England, 1960).

49. Case, K.M. and Zweifel, P.F., *Linear transport theory*, (Addison-Wesley Publishing Co., Reading, MA, 1967).

50. Ishimaru, A., *Wave propagation and scattering in random media*, (Academic Press, New York, NY, 1978).

51. Star, W.M., Diffusion theory of light transport, in *Optical-Thermal Response of Laser-Irradiated Tissue,* eds. Welch, A.J. and van Gemert, M.J.C., pp. 131-206 (Plenum Press, New York, 1995).

52. Wang, L., Jacques, S.L. and Zheng, L., MCML - Monte Carlo modeling of light transport in multi-layered tissues, *Computer Methods and Programs in Biomedicine* **47**, 131-146 (1995).

53. Wang, L. and Jacques, S.L., Monte Carlo modeling of light transport in multi-layered tissues in standard C, (Laser Biology Research Laboratory, M. D. Anderson Cancer Center, University of Texas, Houston, Texas 1992).

54. Keijzer, M. and Hermans, A.J., Light diffusion in stochastically perturbed media, *J. Opt. Soc. Am. A* **10**, 2346-2353 (1993).

55. Patterson, M.S., Chance, B. and Wilson, B.C., Time resolved reflectance and transmittance for the non-invasive measurement of optical properties, *Appl. Opt.* **28**, 2331-2336 (1989).

56. Haskell, R.C., Svaasand, L.O., Tsay, T.-T., Feng, T.-C., McAdams, M.S. and Tromberg, B.J., Boundary conditions for the diffusion equation in radiative transfer, *J. Opt. Soc. Am. A* **11**, 2727-2741 (1994).

57. FEMLAB. Comsol AB, 2004. www.comsol.com.

58. Stokes, G.G., Über die Änderung der Brechbarkeit des Lichtes, *Phil. Transact.* **107**, 11 (1852).

59. Stübel, H., Die Fluoreszenz tierischer Gewebe in ultravioletten Licht, *Pflügers Arch.* **142**, 1 (1911).

60. Policard, A., Etudes sur les aspects offerts par des tumeur experimentales examinée à la lumière de Woods, *CR. Soc. Biol.* **91**, 1423 (1924).

61. Baraga, J.J., Taroni, P., Park, Y.D., An, K., Maestri, A., Tong, L.L., Rava, R.P., Kittrell, C., Dasari, R.R. and Feld, M.S., Ultraviolet laser induced fluorescence of human aorta, *Spectrochim. Acta* **45A**, 95-99 (1989).

62. Chance, B., Cohen, P., Jöbsis, F. and Schoener, B., Intracellular oxidation-reduction states in vivo, *Science* **137**, 499-508 (1962).

63. Chance, B. and Legallais, V., A spectrofluorometer for recording of intracellular oxidation-reduction states, *IEEE Trans. Biomed. Electron.* **BME-10**, 40-47 (1963).

64. Chance, B. and Schoener, B., Fluorometric studies of flavin component of respiratory chain, in *Flavins and flavoproteins,* ed. Slater, pp. 510-519 (Elsevier Publishing Comp, New York, USA, 1966).

65. Sanderson, D.R., Fontana, R.S., Lipson, R.L. and Baldes, E.J., Haematoporphyrin as a diagnostic tool - a preliminary report of new techniques, *Cancer* **30**, 1368-1372 (1972).

66. Kelly, J.F. and Snell, M.E., Haematoporphyrin derivative: a possible aid in the diagnosis and therapy of carcinoma in the bladder, *J. Urol.* **115**, 150-151 (1976).

67. Cortese, D.A., Kinsey, J.H., Woolner, L.B., Payne, W.S., Sanderson, D.R. and Fontana, R.S., Clinical application of a new endoscopic technique for detection of in situ bronchial carcinoma, *Mayo Clin. Proc.* **54**, 635-642 (1979).

68. Profio, A.E., Doiron, D.R. and Sarnaik, J., Fluorometer for endoscopic diagnosis of tumors, *Med. Phys.* **11**, 516-520 (1984).

69. Andersson, P.S., Montán, S. and Svanberg, S., Multi-spectral system for medical fluorescence imaging, *IEEE J. Quant. Electr.* **QE-23**, 1798-1805 (1987).

70. Andersson-Engels, S., Ankerst, J., Johansson, J., Svanberg, K. and Svanberg, S., Tumour marking properties of different haematoporphyrins and tetrasulphonated phthalocyanine - a comparison, *Lasers Med. Sci.* **4**, 115-123 (1989).

71. Brand, S., Stepp, H., Ochsenkuhn, T., Baumgartner, R., Baretton, G., Holl, J., von Ritter, C., Paumgartner, G., Sackmann, M. and Baumgartner, G., Detection of colonic dysplasia by light-induced fluorescence endoscopy: a pilot study, *Int. J. Colorectal. Dis* **14**, 63-68 (1999).

72. Zaak, D., Kriegmair, M., Stepp, H., Baumgartner, R., Oberneder, R.,

Schneede, P., Corvin, S., Frimberger, D., Knuchel, R. and Hofstetter, A., Endoscopic detection of transitional cell carcinoma with 5-aminolevulinic acid: results of 1012 fluorescence endoscopies, *Urology* **57**, 690-694 (2001).

73. Poon, W.S., Schomacker, K.T., Deutsch, T.F. and Martuza, R.L., Laser-induced fluorescence: experimental intraoperative delineation of tumour resection margins, *J. Neurosurg.* **76**, 679-686 (1992).

74. D'Hallewin, M.A., Baert, L. and Vanherzeele, H., Fluorescence imaging of bladder cancer, *Acta Urol. Belg.* **62**, 49-52 (1994).

75. Doiron, D.R., Profio, E., Vincent, R.G. and Dougherty, T.J., Fluorescence bronchoscopy for detection of lung cancer, *Chest* **76**, 27-32 (1979).

76. Eker, C., Montán, S., Jaramillo, E., Koizumi, K., Rubio, C., Andersson-Engels, S., Svanberg, K., Svanberg, S. and Slezak, P., Clinical spectral characterisation of colonic mucosal lesions using autofluorescence and δ aminolevulinic acid sensitisation, *Gut* **44**, 511-518 (1999).

77. Badizadegan, K., Backman, V., Boone, C.W., Crum, C.P., Dasari, R.R., Georgakoudi, I., Keefe, K., Munger, K., Shapshay, S.M., Sheets, E.E. and Feld, M.S., Spectroscopic diagnosis and imaging of invisible pre-cancer, *Faraday Discussions* **126**, 265-279 (2004).

78. Ramanujam, N., Mitchell, M.F., Mahadevan, A., Thomsen, S., Silva, E. and Richards-Kortum, R., Fluorescence spectroscopy: a diagnostic tool for cervical intraepithelial neoplasia (CIN), *Gynecol. Oncol.* **52**, 31-38 (1994).

79. Johansson, J., Fluorescence spectroscopy for medical and environmental diagnostics, Dissertation thesis, Lund Institute of Technology, Lund, Sweden (1993).

80. Rava, R.P., Richards-Kortum, R., Fitzmaurice, M., Cothren, R., Petras, R., Sivak, M., Levin, H. and Feld, M.S., Early detection of dysplasia in colon and bladder tissue using laser induced fluorescence, in *Optical Methods for Tumor Treatment and Early Diagnosis: Mechanisms and Techniques*, ed. Dougherty, T.J., Proc. SPIE vol. **1426**, 68-78 (1991).

81. Andersson-Engels, S. and Wilson, B.C., *In vivo* fluorescence in clinical oncology: Fundamental and practical issues, *J. Cell Pharmacol.* **3**, 48-61 (1992). Invited paper.

82. Logovinsky, V., Kaposi, A.D. and Vanderkooi, J.M., Fluorescence line narrowing spectroscopy of Zn porphyrins, *Photochem. Photobiol.* **57**, 235-241 (1993).

83. Alberts, B., Bray, D., Lewis, J., Raff, M., Roberts, K. and Watson, J.D., *Molecular Biology of the Cell*, 3rd ed., (Garland Publishing Inc., New York, USA, 1994).

84. Thomsen, S. and Tatman, D., Physiological and pathological factors of human breast disease that can influence optical diagnosis, *Ann. N. Y. Acad. Sci.* **838**, 171-193 (1998).

85. Lohmann, W., Mussmann, J., Lohmann, C. and Künzel, W., Native fluorescence of the cervix uteri as a marker for dysplasia and invasive carcinoma, *Eur. J. Obstet. Gynecol. Reprod. Biol.* **31**, 249-253 (1989).

86. af Klinteberg, C., Enejder, A.M.K., Wang, I., Andersson-Engels, S., Svanberg, S. and Svanberg, K., Kinetic fluorescence studies of 5-aminolaevulinic acid-induced proto-

porphyrin IX accumulation in basal cell carcinomas, *J. Photochem. Photobiol. B.* **49**, 120-128 (1999).

87. Nordstrom, R.J., Burke, L., Niloff, J.M. and Myrtle, J.F., Identification of cervical intraepithelial neoplasia (CIN) using UV-excited fluorescence and diffuse-reflectance tissue spectroscopy, *Lasers Surg. Med.* **29**, 118-127 (2001).

88. Benson, R.C., Meyer, R.A., Zaruba, M.E. and McKhann, G.M., Cellular autofluorescence - is it due to flavins?, *J. Histochem. Cytochem.* **27**, 44-48 (1979).

89. Harris, D.M. and Wekhaven, J., Endogenous porphyrin fluorescence in tumors, *Lasers Surg. Med.* **7**, 467-472 (1987).

90. Yang, Y., Ye, Y., Li, F., Li, Y. and Ma, P., Characteristic autofluorescence for cancer diagnosis and its origin, *Lasers Surg. Med.* **7**, 528-532 (1987).

91. Ghadially, F.N., Neish, W.J.P. and Dawkins, H.C., Mechanisms involved in the production of red fluorescence of human and experimental tumors, *J. Path. Bact.* **85**, 77-92 (1963).

92. Reddi, E., Segalla, A., Jori, G., Kerrigan, P.K., Liddell, P.A., Moore, A.L., Moore, T.A. and Gust, D., Carotenoporphyrins as selective photodiagnostic agents for tumors, *Br. J. Cancer* **69**, 40-45 (1994).

93. Nilsson, H., Johansson, J., Svanberg, K., Svanberg, S., Jori, G., Reddi, E., Segalla, A., Gust, D., Moore, A.L. and Moore, Th.A., Laser-induced fluorescence in malignant and normal tissue in mice injected with two different carotenoporphyrins, *Br. J. Cancer* **70**, 873-879 (1994).

94. Takemura, T., Nakajima, S. and Sakata, I., Tumor-localizing fluorescent diagnostic agents without phototoxicity, *Photochem. Photobiol.*

59, 366-370 (1994).

95. Regula, J., MacRobert, A.J., Gorchein, A., Buonaccorsi, G.A., Thorpe, S.M., Spencer, G.M., Hatfield, A.R. and Bown, S.G., Photosensitisation and photodynamic therapy of oesophageal, duodenal and colorectal tumours using 5 aminolaevulinic acid induced protoporphyrin IX - a pilot study, *Gut* **36**, 67-75 (1995).

96. Heyerdahl, H., Wang, I., Liu, D.L., Berg, R., Andersson-Engels, S., Peng, Q., Moan, J., Svanberg, S. and Svanberg, K., Pharmacokinetic studies on 5-aminolevulinic acid-induced protoporphyrin IX accumulation in tumours and normal tissues, *Cancer Lett.* **112**, 225-231 (1997).

97. Leibovici, L., Schoenfeld, N., Yehoshua, H.A., Mamet, R., Rakowski, E., Shindel, A. and Atsmon, A., Activity of porphobilinogen deaminase in peripheral blood mononuclear cells of patients with metastatic cancer, *Cancer* **62**, 2297-2300 (1988).

98. Kondo, M., Hirota, N., Takaoka, T. and Kajiwara, M., Heme-biosynthetic enzyme activities and porphyrin accumulation in normal liver and hepatoma cell lines of rat, *Cell Biol. Toxicol.* **9**, 95-105 (1993).

99. Hinnen, P., de Rooij, F.W.M., van Velthuysen, M.L.F., Edixhoven, A., van Hillegersberg, R., Tilanus, H.W., Wilson, J.H.P. and Siersema, P.D., Biochemical basis of 5-aminolaevulinic acid-induced protoporphyrin IX accumulation: a study in patients with (pre)malignant lesions of the oesophagus, *Br. J. Cancer* **78**, 679-682 (1998).

100. El-Sharabasy, M.M.H., El-Waseef, A.M., Hafez, M.M. and Salim, S.A., Porphyrin metabolism in some malignant diseases, *Br. J. Cancer* **65**,

409-412 (1992).

101. van Hillegersberg, R., van den Berg, J.W.O., Kort, W.J., Terpstra, O.T. and Wilson, J.H.P., Selective accumulation of endogenously produced porphyrins in a liver metastasis model in rats, *Gastroenterology* **103**, 647-651 (1992).

102. Dailey, H.A. and Smith, A., Differential interaction of porphyrins used in photoradiation therapy with ferrochelatase, *Biochem. J.* **223**, 441-445 (1984).

103. Kennedy, J.C., Pottier, R.H. and Pross, D.C., Photodynamic therapy with endogenous protoporphyrin IX: Basic principles and present clinical experience, *J. Photochem. Photobiol. B.* **6**, 143-148 (1990).

104. Goff, B.A., Bachor, R., Kollias, N. and Hasan, T., Effects of photo-dynamic therapy with topical application of 5-aminolevulinic acid on normal skin of hairless guinea pigs, *J. Photochem. Photobiol. B.* **15**, 239-251 (1992).

105. van den Akker, J.T.H.M., Iani, V., Star, W.M., Sterenborg, H.J.C.M. and Moan, J., Topical application of 5-aminolevulinic acid hexyl ester and 5-aminolevulinic acid to normal nude mouse skin: Differences in proto-porphyrin IX fluorescence kinetics and the role of the stratum corneum, *Photochem. Photobiol.* **72**, 681-689 (2000).

106. Rhodes, L.E., Tsoukas, M.M., Anderson, R.R. and Kollias, N., Iontophoretic delivery of ALA provides a quantitative model for ALA pharmacokinetics and PpIX phototoxicity in human skin, *J. Invest. Dermatol.* **108**, 87-91 (1997).

107. Peng, Q., Moan, J., Warloe, T., Iani, V., Steen, H.B., Bjørseth, A. and Nesland, J.M., Build-up of esterified aminolevulinic-acid-derivative-induced porphyrin fluorescence in normal mouse skin, *J. Photochem. Photobiol. B.* **34**, 95-96 (1996).

108. Uehlinger, P., Zellweger, M., Wagnieres, G., Juillerat-Jeanneret, L., van den Bergh, H. and Lange, N., 5-Aminolevulinic acid and its derivatives: physical chemical properties and protoporphyrin IX formation in cultured cells, *J. Photochem. Photobiol. B.* **54**, 72-80 (2000).

109. Juzeniene, A., Juzenas, P., Iani, V. and Moan, J., Topical application of 5-aminolevulinic acid and its methyl-ester, hexylester and octylester derivatives: Considerations for dosimetry in mouse skin model, *Photochem. Photobiol.* **76**, 329-334 (2002).

110. Kloek, J. and Beijersbergen van Henegouwen, G.M.J., Prodrugs of 5-aminolevulinic acid for photodynamic therapy, *Photochem. Photobiol.* **64**, 994-1000 (1996).

111. Kloek, J., Akkermans, W. and Beijersbergen van Henegouwen, G.M.J., Derivatives of 5-amino-levulinic acid for photodynamic therapy: enzymatic conversion into protoporphyrin, *Photochem. Photobiol.* **67**, 150-154 (1998).

112. Eker, C., Optical characterization of tissue for medical diagnostics, Dissertation thesis, Lund Institute of Technology, Lund, Sweden (1999).

113. Balchum, O.J., Profio, A.E., Doiron, D.R. and Huth, G.C., Imaging fluorescence bronchoscopy for localizing early bronchial cancer and carcinoma in situ, in *Porphyrin localization and treatment of tumors,* eds. Doiron, D.R. and Gomer, C.J., pp. 847-861 (Alan R. Liss, Inc., New York, USA, 1984).

114. Cubeddu, R., Canti, G., Taroni, P. and Valentini, G., Time-gated fluorescence imaging for the diagnosis of tumors in a murine model, *Photochem. Photobiol.* **57**, 480-485 (1993).

115. Andersson-Engels, S., Canti, G., Cubeddu, R., Eker, C., af Klinteberg, C., Pifferi, A., Svanberg, K., Svanberg, S., Taroni, P., Valentini, G. and Wang, I., Preliminary evaluation of two fluorescence imaging methods for detection of basal cell carcinomas of the skin, *Lasers Surg. Med.* **26**, 76-82 (2000).

116. af Klinteberg, C., Andreasson, M., Sandström, O., Andersson-Engels, S. and Svanberg, S., Compact medical fluorosensor for minimally invasive tissue characterisation, Submitted (2003).

117. Gustafsson, U., Pålsson, S. and Svanberg, S., Compact fibre-optic fluorosensor using a continuous wave violet diode laser and an integrated spectrometer, *Rev. Sci. Instrum.* **71**, 3004-3006 (2000).

118. Ekström, J., Development of software for a diode-based fluorosensor, Master thesis, Department of Physics, Lund Institute of Technology, Lund, Sweden (2002).

119. Andersson-Engels, S., Svanberg, K. and Svanberg, S., Fluorescence imaging in medical diagnostics, in *Biomedical Optics,* (, 2003).

120. Andersson-Engels, S., Johansson, J. and Svanberg, S., Medical diagnostic system based on simultaneous multi-spectral fluorescence imaging, *Appl. Opt.* **33**, 8022-8029 (1994).

121. Svanberg, K., Wang, I., Colleen, S., Idvall, I., Ingvar, C., Rydell, R., Jocham, D., Diddens, H., Bown, S., Gregory, G., Montán, S., Andersson-Engels, S. and Svanberg, S., Clinical multi-colour fluorescence imaging of malignant tumours - initial experience, *Acta Radiol.* **39**, 2-9 (1998).

122. Ehsan, A., Sommer, F., Haupt, G. and Engelmann, U., Significance of fluorescence cystoscopy for diagnosis of superficial bladder cancer after intravesical instillation of delta aminolevulinic acid, *Urol. Int.* **67**, 298-304 (2001).

123. Kriegmair, M., Stepp, H., Steinbach, P., Lumper, W., Ehsan, A., Stepp, H.G., Rick, K., Knuchel, R., Baumgartner, R. and Hofstetter, A., Fluorescence cystoscopy following intravesical instillation of 5-aminolevulinic acid: a new procedure with high sensitivity for detection of hardly visible urothelial neoplasias, *Urol. Int.* **55**, 190-196 (1995).

124. Leunig, A., Rick, K., Stepp, H., Gutmann, R., Alwin, G., Baumgartner, R. and Feyh, J., Fluorescence imaging and spectroscopy of 5-aminolevulinic acid induced protoporphyrin IX for the detection of neoplastic lesions in the oral cavity, *Am. J. Surg.* **172**, 674-677 (1996).

125. Betz, C.S., Stepp, H., Janda, P., Arbogast, S., Grevers, G., Baumgartner, R. and Leunig, A., A comparative study of normal inspection, autofluorescence and 5-ALA-induced PPIX fluorescence for oral cancer diagnosis, *Int. J. Cancer* **97**, 245-252 (2002).

126. Ladner, D.P., Steiner, R.A., Allemann, J., Haller, U. and Walt, H., Photodynamic diagnosis of breast tumours after oral application of aminolevulinic acid, *Br. J. Cancer* 33-37 (2001).

127. Hillemanns, P., Weingandt, H., Baumgartner, R., Diebold, J., Xiang, W. and Stepp, H., Photodetection of cervical intraepithelial neoplasia using

5-aminolevulinic acid-induced porphyrin fluorescence, *Cancer* **88**, 2275-2282 (2000).

128. Gahlen, J., Prosst, R.L., Pietschmann, M., Rheinwald, M., Haase, T. and Herfarth, C., Spectrometry supports fluorescence staging laparoscopy after intraperitoneal aminolaevulinic acid lavage for gastrointestinal tumours, *J. Photochem. Photobiol. B.* **52**, 131-135 (1999).

129. Garini, Y., Katzir, N., Cabib, D., Buckwald, R., Soenksen, D.G. and Malik, Z., Spectralbio-imaging, in *Fluorescence imaging spectroscopy and microscopy,* eds. Wang, X.F. and Herman, B., pp. 88-124 (, 1996).

130. Malik, Z., Dishi, M. and Garini, Y., Fourier transform multipixel spectroscopy and spectral imaging of protoporphyrin in single melanoma cells, *Photochem. Photobiol.* **63**, 608-614 (1996).

131. Schomacker, K.T., Frisoli, J.K., Compton, C.C., Flotte, T.J., Richter, J.M., Nishioka, N.S. and Deutsch, T.F., Ultraviolet laser-induced fluorescence of colonic tissue: Basic biology and diagnostic potential, *Lasers Surg. Med.* **12**, 63-78 (1992).

132. Fraunfelder, F.T., Zacarian, S.A., Wingfield, D.L. and Limmer, B.L., Results of cryotherapy for eyelid malignancies, *Am. J. Ophthalmol.* **97**, 184-188 (1984).

133. Andersson, P.S., Gustafson, A., Stenram, U., Svanberg, K. and Svanberg, S., Diagnosis of arterial atherosclerosis using laser-induced fluorescence, *Lasers Med. Sci.* **2**, 261-266 (1987).

134. Richards-Kortum, R., Rava, R.P., Fitzmaurice, M., Tong, L.L., Ratliff, N.B., Kramer, J.R. and Feld, M.S., A one-layer model of laser-induced fluorescence for diagnosis of disease in human tissue: applications to atherosclerosis, *IEEE Trans. Biomed. Eng.* **36**, 1222-1232 (1989).

135. Sinaasappel, M. and Sterenborg, H.J.C.M., Quantification of the hematoporphyrin derivative by fluorescence measurement using dual-wavelength excitation and dual-wavelength detection, *Appl. Opt.* **32**, 541-548 (1993).

136. Foote, C.S., Definition of Type-I and Type-Ii Photosensitized Oxidation, *Photochem. Photobiol.* **54**, 659 (1991).

137. Orenstein, A., Kostenich, G., Tsur, H., Kogan, L. and Malik, Z., Temperature monitoring during photodynamic therapy of skin tumors with topical 5-aminolevulinic acid application, *Cancer Lett.* **93**, 227-232 (1995).

138. Morton, C.A., Brown, S.B., Collins, S., Ibbotson, S., Jenkinson, H., Kurwa, H., Langmack, K., Mckenna, K., Moseley, H., Pearse, A.D., Stringer, M., Taylor, D.K., Wong, G. and Rhodes, L.E., Guidelines for topical photodynamic therapy: report of a workshop of the British Photodermatology Group, *Br. J. Dermatol.* **146**, 552-567 (2002).

139. Brown, S.B., Brown, E.A. and Walker, I., The present and future role of photodynamic therapy in cancer treatment, *Lancet Oncology* **5**, 497-508 (2004).

140. Weishaupt, K.R., Gomer, C.J. and Dougherty, T.J., Identification of singlet oxygen as the cytotoxic agent in photo-inactivation of a murine tumor, *Cancer Res.* **36**, 2326-2329 (1976).

141. Henderson, B.W. and Dougherty, T.J., How does photodynamic therapy work?, *Photochem. Photobiol.* **55**, 145-157 (1992).

142. Oleinick, N.L., Morris, R.L. and Belichenko, T., The role of apoptosis in response to photodynamic therapy: what, where, why, and how, *Photochem. Photobiol. Sci.* **1**, 1-21 (2002).

143. Lilge, L., Portnoy, M. and Wilson, B.C., Apoptosis induced in vivo by photodynamic therapy in normal brain and intracranial tumour tissue, *Br. J. Cancer* **83**, 1110-1117 (2000).

144. Stewart, F., Baas, P. and Star, W., What does photodynamic therapy have to offer radiation oncologists (or their cancer patients)?, *Radiothermal Oncology* **48**, 233-248 (1998).

145. Diamond, I., Granelli, S.G., McDonagh, A.F., Nielsen, S.F., Wilson, C.B. and Jaenicke, R., Photo-dynamic therapy of malignant tumours, *Lancet* **2**, 1175-1177 (1972).

146. Dougherty, T.J., Kaufman, J.E., Goldfarb, A., Weishaupt, K.R., Boyle, D. and Mittleman, A., Photoradiation therapy for the treatment of malignant tumors, *Cancer Res.* **38**, 2628-2635 (1978).

147. Dougherty, T.J., Photoradiation therapy for cutaneous and sub-cutaneous malignancies, *J. Invest. Dermatol.* **77**, 122-124 (1981).

148. Malik, Z. and Lugaci, H., Destruction of erythroleukaemic cells by photoinactivation of endogenous porphyrins, *Br. J. Cancer* **56**, 589-595 (1987).

149. Peng, Q., Evensen, J.F., Rimington, C. and Moan, J., A comparison of different photosensitizing dyes with respect to uptake C3H-tumors and tissues of mice, *Cancer Lett.* **36**, 1-10 (1987).

150. Kennedy, J.C. and Pottier, R.H., Endogenous protoporphyrin IX, a clinically useful photosensitizer for photodynamic therapy, *J. Photochem. Photobiol. B.* **14**, 275-292 (1992).

151. Svanberg, K., Andersson, T., Killander, D., Wang, I., Stenram, U., Andersson-Engels, S., Berg, R., Johansson, J. and Svanberg, S., Photodynamic therapy of non-melanoma malignant tumours of the skin using topical δ-amino levulinic acid sensitization and laser irradiation, *Br. J. Dermatol.* **130**, 743-751 (1994).

152. Lichtenthaler, H.K. and Rinderle, U., *The role of chlorophyll fluorescence in the detection of stress conditions in plants*, (, 1988).

153. Kubler, A.C., Haase, T., Staff, C., Kahle, B., Rheinwald, M. and Muhling, J., Photodynamic therapy of primary nonmelanomatous skin tumours of the head and neck, *Lasers Surg. Med.* **25**, 60-68 (1999).

154. Kubler, A.C., de Carpentier, J., Hopper, C., Leonard, A.G. and Putnam, G., Treatment of squamous cell carcinoma of the lip using Foscan-mediated Photodynamic Therapy, *International Journal of Oral and Maxillofacial Surgery* **30**, 504-509 (2001).

155. Baas, P., Saarnak, A.E., Oppelaar, H., Neering, H. and Stewart, F.A., Photodynamic therapy with *meta*-tetrahydroxyphenylchlorin for basal cell carcinoma: a phase I/II study, *Br. J. Dermatol.* **145**, 75-78 (2001).

156. Arnold, J. et al., Verteporfin therapy of subfoveal choroidal neovascular-ization in age-related macular degeneration: Two-year results of a randomized clinical trial including lesions with occult with no classic choroidal neovascularization-verte-porfin in photodynamic therapy report 2, *Am. J. Ophthalmol.* **131**, 541-560 (2001).

157. Renno, R.Z. and Miller, J.W., Photosensitizer delivery for photodynamic therapy of choroidal neovascularization, *Advanced Drug Delivery Reviews* **52**, 63-78 (2001).

158. Müller, S., Walt, H., Dobler-Girdziunaite, D., Fiedler, D. and Haller, U., Enhanced photodynamic effects using fractionated laser light, *J. Photochem. Photobiol.* **42**, 67-70 (1998).

159. Curnow, A., McIlroy, B.W., Postle-Hacon, M.J., MacRobert, A.J. and Bown, S.G., Light dose fractionation to enhance photodynamic therapy using 5-aminolevulinic acid in the normal rat colon, *Photochem. Photobiol.* **69**, 71-76 (1999).

160. Robinson, D.J., de Bruijn, H.S., Wolf, W.J., Sterenborg, H.J.C.M. and Star, W.M., Topical 5-aminolevulinic acid-photodynamic therapy of hairless mouse skin using two-fold illumination schemes: PpIX fluorescence kinetics, photobleaching and biological effect, *Photochem. Photobiol.* **72**, 794-802 (2000).

161. Thissen, M.R., de Blois, M.W., Robinson, D.J., de Bruijn, H.S., Dutrieux, R.P. and Star, W.M., PpIX fluorescence kinetics and increased skin damage after intracutaneous injection of 5-aminolevulinic acid and repeated illumination, *J. Invest. Dermatol.* **118**, 239-245 (2002).

162. Robinson, D.J., de Bruijn, H.S., Star, W.M. and Sterenborg, H.J.C.M., Dose and timing of the first light fraction in two-fold illumination schemes for topical ALA-mediated photodynamic therapy of hairless mouse skin, *Photochem. Photobiol.* **77**, 319-323 (2003).

163. Babilas, P., Schacht, V., Liebsch, G., Wolfbeis, O.S., Landthaler, M., Szeimies, R.-M. and Abels, C., Effects of light fractionation and different fluence rates on photodynamic therapy with δ-aminolaevulinic acid *in vivo*, *Br. J. Cancer* **88**, 1462-1469 (2003).

164. Svaasand, L.O., Photodynamic and photohyperthermic response of malignant tumors, *Med. Phys.* **12**, 455-461 (1985).

165. Brown, S.B., The role of light in the treatment of non-melanoma skin cancer using methyl aminolevulinate, *J. Dermatol. Treat.* **14**, 11-14 (2003).

166. Foley, P., Clinical efficacy of methyl aminolevulinate (Metvix®) photo-dynamic therapy, *J. Dermatol. Treat.* **14**, 15-22 (2003).

167. Whitehurst, C., Pantelides, M.L., Moore, J.V. and Blacklock, N.J., Optimization of multifiber light delivery for the photodynamic therapy of localized prostate cancer, *Photochem. Photobiol.* **58**, 589-593 (1993).

168. Soler, A.M., Angell-Petersen, E., Warloe, T., Tausjo, J., Steen, H.B., Moan, J. and Giercksky, K.E., Photodynamic therapy of superficial basal cell carcinoma with 5-aminolevulinic acid with dimethyl-sulfoxide and ethylendiaminetetra-acetic acid: A comparison of two light sources, *Photochem. Photobiol.* **71**, 724-729 (2000).

169. Lowdell, C.P., Ash, D.V., Driver, I. and Brown, S.B., Interstitial photodynamic therapy. Clinical experience with diffusing fibres in the treatment of cutaneous and subcutaneous tumours, *Br. J. Cancer* **67**, 1398-1403 (1993).

170. Purkiss, S.F., Dean, R., Allardice, J.T., Grahn, M. and Williams, N.S., An interstitial light delivery system for photodynamic therapy within the liver, *Lasers Med. Sci.* **8**, 253-257 (1993).

171. Chang, S.C., Buonaccorsi, G., MacRobert, A. and Bown, S.G., Interstitial and transurethral photo-dynamic therapy of the canine prostate using meso-tetra-(m-hydroxyphenyl) chlorin, *Int. J. Cancer* **67**, 555-562 (1996).

172. Lou, P.J., Jager, H.R., Jones, L., Theodossy, T., Bown, S.G. and Hopper, C., Interstitial photodynamic therapy as salvage treatment for recurrent head and neck cancer, *Br. J. Cancer* **91**, 441-446 (2004).

173. Nilsson, N.J., Oximetry, *Physiological Reviews* **40**, 1-26 (1960).

174. Bowes, W.A., III, Corke, B.C. and Hulka, J., Pulse oximetry: A review of the theory, accuracy, and clinical applications, *Obstet. Gynecol.* **74**, 541-546 (1989).

175. Oberg, P.A., Optical Sensors in Medical Care, *Sensors Update* **13**, 201-232 (2003).

176. Soumya, M. and Foster, T.H., Carbogen breathing significantly enhances the penetration of red light in murine tumours *in vivo*, *Phys. Med. Biol.* **49**, 1891-1904 (2004).

177. Boere, I.A., Robinson, D.J., de Bruijn, H.S., van den Boogert, J., Tilanus, H.W., Sterenborg, H.J.C.M. and de Bruin, R.W.F., Monitoring In Situ Dosimetry and Protoporphyrin IX Fluorescence Photobleaching in the Normal Rat Esophagus During 5-Aminolevulinic Acid Photodynamic Therapy, *Photochem. Photobiol.* **78**, 271-2 (2003).

178. Wilson, B.C., Patterson, M.S. and Lilge, L., Implicit and explicit dosimetry in photodynamic therapy: a new paradigm, *Lasers Med. Sci.* **12**, 182-199 (1997).